JOURNAL OF GEOPHYSICAL RESEARCH, VOL. 105, NO. A11, PAGES 25,265–25,290, NOVEMBER 1, 2000

Electromagnetics of substorm onsets in the near-geosynchronous plasma sheet

G. M. Erickson[1] N. C. Maynard,[2] W. J. Burke,[3] G. R. Wilson,[2]
and M. A. Heinemann[3]

Abstract. A search of the CRRES database identified 20 events in which the satellite was located within the local-time sector spanned by the substorm current wedge (SCW) as it formed. Poynting vectors for low-frequency waves are derived from the electric and magnetic field measurements. In 19 of the events, data are inconsistent with the notion that the SCW initiates from the braking of earthward bulk flows emanating from a near-Earth X line. Rather, the data support drift-Alfvén ballooning in the near-geosynchronous plasma sheet as being responsible for initiation of the SCW and substorm onset. Dipolarization at CRRES is preceded by eastward excursions of the electric field (trigger waves), at which time the first significant electromagnetic energy is observed flowing toward the ionosphere. Dipolarization and the SCW appear before ground onset, following one or more of these trigger waves. The so-called "explosive growth phase" occurs in association with explosive growth of the trigger waves soon after onset. Seven characteristic features of substorm onsets and expansions observed at CRRES are described. Among these are two stages of expansion. The first expansion stage is initiated by the trigger waves (ballooning) in the near-geosynchronous plasma sheet. Approximately 10 minutes later a second stage begins consistent with the arrival of earthward bulk flows emanating from a near-Earth X line. Near-geosynchronous substorm onsets can explain the observed increase in the occurrence rate of fast bulk flows earthward of its minimum value near $X = -12\ R_E$. Drift-Alfvén ballooning also provides a possible causal link between observed reductions of the solar wind driver and substorm onsets.

1. Introduction

From the perspective of Earth's magnetotail, there are two key events in the evolution of a substorm: (1) initiation of the substorm current wedge (SCW) in the near-geosynchronous plasma sheet and (2) the onset of magnetic reconnection in the near-Earth to midtail plasma sheet. The SCW appears at substorm onset when cross-tail current shunts through the ionosphere as a westward electrojet [*Fairfield and Ness*, 1970; *McPherron et al.*, 1973], producing Pi2 oscillations [*Rostoker and Olson*, 1979] and onset of a magnetic bay at nearby ground magnetometer stations [*Heppner*, 1958]. Magnetic reconnection accounts for the rapid release of lobe flux stored in the tail during the growth phase and poleward expansion of the auroral bulge into the polar cap [*Hones*, 1979; *Russell and McPherron*, 1973]. Depending on where in the plasma sheet a satellite is situated, one or the other of these key processes dominates the observations. It is not surprising then that two basic models of substorm onset and expansion have been pursued: the near-geosynchronous onset (NGO) and the near-Earth neutral line (NENL) models. (The NGO model is essentially the synthesis near-Earth current disruption model described by *Lui* [1991].) The causal link between the two key tail substorm events in these two models is shown schematically in Figure 1. Both the NGO and the NENL models recognize near-Earth reconnection as an essential part of the substorm expansion process. They are distinguished by whether or not reconnection in the near-Earth tail is a trigger or an event subsequent to substorm onset. *Siscoe* [1993], *Erickson* [1995], and *Vasyliunas* [1998] provide reviews of physical requirements for the two models.

Near-geosynchronous plasma-sheet observations favor the NGO model, in which initiation of the SCW results from onset of a nearby instability and disruption of cross-tail current. Suggestions for that instability include a cross-field current instability [*Lui et al.*, 1990] and a magnetosphere-ionosphere (M-I) coupling

[1]Center for Space Physics, Boston University, Boston, Massachusetts.
[2]Mission Research Corporation, Nashua, New Hampshire.
[3]Air Force Research Laboratory, Hanscom Air Force Base, Massachusetts.

Paper number 1999JA000424.
0148-0227/00/1999JA000424$09.00

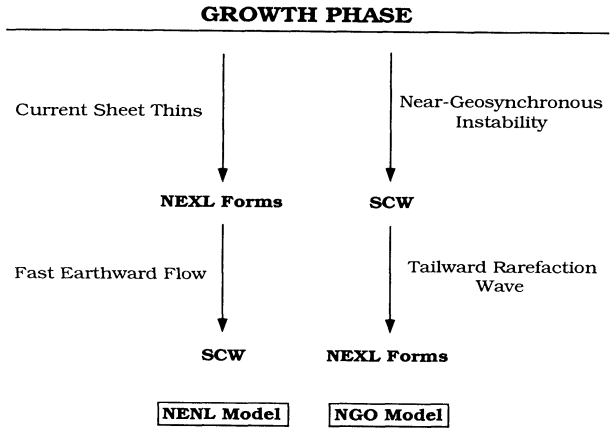

Figure 1. The causal link between near-Earth X line (NEXL) formation and the substorm current wedge (SCW) within the two substorm hypotheses: (left) the near-Earth neutral line (NENL) model and (right) the near-geosynchronous onset (NGO) model.

feedback instability [*Kan*, 1993]. However, ballooning, perhaps coupled to the aforementioned processes, appears consistent with near-geosynchronous observations of substorm onsets. *Roux et al.* [1991] invoked drift-Alfvén ballooning (DAB) to explain the observation of electric field oscillations and successive field-aligned current (FAC) filaments of alternating direction passing over the GEOS 2 spacecraft during a substorm expansion. Using conjugate ground observations, they related ballooning waves to westward traveling surges (WTSs). *Holter et al.* [1995] performed spectral and wavelet analyses to characterize the transient oscillations observed during the Roux et al. event. *Elphinstone et al.* [1995] described azimuthally spaced auroral forms usually present prior to the explosive poleward motion associated with optical substorm onset. They suggest that they are growth phase activities causally related to substorm onset, specifically Alfvén ballooning.

Pu et al. [1997] used two-fluid MHD to derive ballooning criteria. They found two unstable drift-ballooning-mode (DBM) solutions, DBM1 and DBM2, which correspond to the solutions of *Ohtani and Tamao* [1993] and *Miura et al.* [1989], respectively. Using GEOS 2 observations to infer plasma and magnetic field characteristics preceding 16 isolated substorm onsets, they found that the necessary conditions for DBM2 were fulfilled in 14 of the events. *Hurricane et al.* [1999] analyzed drift-Alfvén ballooning and suggest that the nonlinear phase amplitude can grow explosively into narrow fingers to simultaneously destabilize the surrounding configuration. They termed this process "substorm detonation."

Associated with local onsets in the near-geosynchronous plasma sheet are the so-called "explosive-growth-phase" (EGP) signatures. *Ohtani et al.* [1992] analyzed the behavior of magnetic fields and energetic particles from the Active Magnetospheric Particle Tracer Explorers/Charge Composition Explorer (AMPTE/CCE) spacecraft in the near-geosynchronous plasma sheet ($R \leq 9\ R_E$) just prior to the sharp recovery in the magnetic H component and the beginning of current disruption. During an EGP interval, AMPTE/CCE detected (1) a sharp depression of the magnetic H component, (2) increased flux of duskward flowing energetic ions, and (3) an increase in the magnitude of the magnetic V (radial) component. Ohtani et al. interpreted these signatures as resulting from an explosive increase of the cross-tail current tailward of the satellite. *Cheng and Lui* [1998] derive a kinetic ballooning instability and suggest that it can account for EGP and current disruption signatures observed in the near-geosynchronous plasma sheet.

In NGO morphology the formation of a near-Earth X line (NEXL) occurs during the expansion phase. It is unclear how onset in the near-geosynchronous region causes the NEXL to form downtail. One suggestion is that as the cross-tail current is reduced, dipolarization ensues, leaving a plasma pressure reduction in its wake. This causes the plasma sheet to pinch as the pressure reduction propagates downtail as a rarefaction wave [*Chao et al.*, 1977; *Lui*, 1978]. At some point, this process activates one or more NEXLs in the growth-phase-thinned current sheet.

A branch of the NGO morphology is the substorm model postulated by *Lyons* [1995]. Repeated investigations support the notion that a large percentage of substorm onsets are triggered by reduction of the solar wind driver [see, e.g., *Rostoker*, 1983; *McPherron et al.*, 1986]. Lyons suggests that all substorms are triggered in this manner. However, observations indicate that some substorms occur in the absence of an external trigger [e.g., *Henderson et al.*, 1996].

Beyond the near-geosynchronous region, observations favor the NENL model in which magnetic reconnection in the midtail plasma sheet is responsible for substorm onset. In the plasma sheet 15–60 R_E downtail, substorm expansions are identified from activation of a NEXL [*Nagai and Machida*, 1998], evidenced by fast flows, bipolar magnetic field signatures, and creation of one or more plasmoids [e.g., *Moldwin and Hughes*, 1993]. On occasion, NEXL formation has been observed in close temporal proximity to ground onset and even a few minutes before [e.g., *Sergeev et al.*, 1995; *Ohtani et al.*, 1999]. The SCW results as magnetic flux transported by fast earthward flows emanating from the NEXL piles up (dipolarization) in the inner plasma sheet [*Birn and Hesse*, 1991]. The braking of that flow provides current diversion and power to the ionosphere [*Haerendel*, 1992; *Shiokawa et al.*, 1997]. The resultant field collapse and distortion modify pressure gradients, which provide a more dominant and sustained contribution to the SCW [*Birn et al.*, 1999].

Maynard et al. [1996a] (hereinafter referred to as M96) presented observations from the Chemical Release and Radiation Effects Satellite (CRRES) during six substorms that demonstrate several particle and

field features of substorm onset and early expansion in the near-geosynchronous plasma sheet. The most significant observations were of brief electric field reversals from dawn-dusk to dusk-dawn preceding onsets. In three of the events the alignment of the CRRES electric field booms allowed M96 to compute the third component of $\mathbf{E}$ using the assumption $\mathbf{E} \cdot \mathbf{B} = 0$. This permitted determination of the component of the Poynting vector parallel to the magnetic field for low-frequency electromagnetic waves. Preonset electric field reversals were accompanied by wave power flowing toward the ionosphere. At these times, $\mathbf{j} \cdot \mathbf{E} < 0$ in the inner plasma sheet, and M96 thus assumed a local source of the wave power. Dipolarizations began after the dusk-dawn excursions and prior to westward electric field enhancements and particle injections, characteristic of the substorm expansion phase. Furthermore, the CRRES measurements suggested that coupling between the magnetosphere and ionosphere plays a significant role in determining onset of the expansion phase. On the basis of these observations, M96 suggested a phenomenological model of substorm onset associated with ballooning in the near-geosynchronous plasma sheet in which M-I coupling plays an important role.

In addition to information on coupling to the ionosphere from the parallel Poynting flux, the perpendicular Poynting flux from the waves also reveals information relative to the position of the source. A preliminary report by *Maynard et al.* [1998b] concluded that the primary perpendicular power was azimuthal, limiting the source of onset to the near-geosynchronous plasma sheet. No significant inward flux was observed, which would be necessary if triggering were to be done by a NEXL. It is the purpose of this paper to expand these findings and to order the events surrounding onset into a comprehensive NGO morphology.

We have searched the CRRES database to identify 20 dipolarization events during which the spacecraft was in the plasma sheet near onset's central meridian and the Poynting vector could be computed for low-frequency (<34 mHz) waves. These are listed in Table 1 with ground onset time (and its source) and, the magnitude of the magnetic field at the spacecraft, along with ephemeris information. There were 18 local substorm onsets and two pseudobreakups. Our examination of these events addresses several issues surrounding substorm onsets and expansions. The primary question is suggested in Figure 1: Are substorms initiated by the onset of enhanced reconnection in the near-Earth tail, or do they begin in the near-geosynchronous region with the formation of the SCW? We answer this question by determining if the power released toward the ionosphere within the SCW at onset is associated with braking or acceleration of plasma in the plasma sheet. More generally, we examine whether enhanced wave power, observed in the near-geosynchronous plasma sheet prior

Table 1. Events When CRRES Was Near Onset's Central Meridian

Event	Orbit	Date	Station	Onset, UT	R	L	MLT	B, nT
A	461	Jan. 31	McMurray	0846	6.2	6.6	0041	124
B	481	Feb. 8		1302	6.3	6.6	0000	137
C	484	Feb. 9	*AL*	1653	5.9	6.3	2253	75
D	540[a]	March 4	Dixon		5.5	6.2	2359	225
E	540	March 4	Dixon	1938	5.2	6.1	0003	250
F	545[a]	March 6	IMAGE	1941	6.0	6.7	2308	174
G	545	March 6	*AL*/IMAGE	1952	5.9	6.6	2319	193
H	545	March 6	*AL*/IMAGE	2018	5.6	6.3	2335	213
I	546[b]	March 7	*AL*	0321	6.1	6.7	2159	94
J	547	March 7	Tixie	1320	6.2	6.7	2209	168
K	547	March 7	Tixie	1412	6.3	6.9	2240	153
L	547	March 7	Tixie	1436	6.2	7.0	2247	154
M	550	March 8	Muonio	2112	5.8	6.4	2317	165
N	552	March 9	Tixie	1317	5.4	5.7	2113	143
O	553	March 10			6.3	6.8	2231	120
P	572[b]	March 17	Muonio	2015	6.3	6.9	2215	102
Q	577	March 19	Leirvoguir	2258	5.6	6.2	2304	143
R	583	March 22	College	0825	6.2	6.7	2219	110
S	586[b]	March 23	Tixie	1126	5.4	5.7	2038	164
T	593[c]	March 26	Dawson	0847	5.7	6.1	2053	167

[a]Pseudobreakup.

[b]At the westward edge of onset sector.

[c]Storm time.

to and at the time of SCW formation and onset, arrives from downtail, either directly or reflected from the ionosphere (NENL model), or is generated locally (NGO model). Our near-geosynchronous observations not only favor the NGO onset model, but also directly contradict the predictions of the NENL onset model in 19 of the 20 events. The other event (event T), which occurred during the March 1991 storm, is a candidate for NENL onset. In addition, this investigation sheds light on (1) the origin of Pi2 oscillations and their role in substorm development, (2) the EGP, and (3) the dynamics of regions initially outside the substorm current wedge. Possible resolutions to two other issues are suggested by the results: (1) the curious increase in the occurrence rate of high-speed ion flows within $X = -12$ R_E observed by *Shiokawa et al.* [1997], and (2) solar wind triggering.

The observations surrounding onsets are complex but consistent from one event to the next. Following a brief description of the data sources for this study, an idealized preview of the key observational signatures associated with local onsets in the inner plasma sheet is provided together with corresponding definitions. Two events are examined in detail to illustrate the behavior of the electric and magnetic fields surrounding substorm onsets. Measurements of low-frequency wave power associated with local onsets, which are the main focus of this investigation, as well as other pertinent parameters are given in tabular form for all 20 events. In section 5 we reconsider the two competing phenomenological models of substorm onset and use the observational data to address the issues listed above. On the basis of these findings we suggest a model for substorms with NGO morphology. Section 6 summarizes our observations and major conclusions.

2. Data Sources

The CRRES satellite was launched in July 1990 into an 18.2° inclination orbit with apogee at a geocentric distance of 6.3 R_E and perigee at an altitude of 350 km. The orbital period was about 10 hours. The satellite was spin stabilized, at a rate of 2 rpm, with its spin axis pointing within 15° of the Sun. The local time of apogee, initially at 0800, precessed toward the west at ~0.67° per day. For this investigation we are primarily interested in measurements taken by the electric field instrument (EFI) [*Wygant et al.*, 1992] and the magnetometer [*Singer et al.*, 1992]. In addition, we use measurements from the low-energy plasma analyzer (LEPA) [*Hardy et al.*, 1993] to time injections at CRRES.

CRRES monitored variations in the Earth's magnetic field using a triaxial fluxgate magnetometer mounted at the end of a 6.1-m mast. Two different gain ranges of $\pm 45,000$ and ± 900 nT allowed least significant bit resolution of 22 and 0.4 nT, respectively. The instrument is typically in high-sensitivity mode on all three axes over 75% of each CRRES orbit. The normal sampling rate is 16 s^{-1}.

The electric field instrument on CRRES utilized a biased, double-floating probe technique. Both cylindrical and spherical sensors are located on 100-m tip-to-tip wire antennas, which were biased to optimize the impedance between the probes and the plasma and thus minimize errors. In its optimum range the bias current effectively nulls photoemission currents and minimizes changes in floating potentials for small variations of collection current. This allows the probes to provide accurate electric field measurements even at low plasma densities. Having the spin axis of CRRES point toward the Sun minimized photoemission asymmetries. The two electric field measurement axes are in the spin plane, approximately aligned with the solar-ecliptic Y and Z directions. The third component can be derived using the $\mathbf{E} \cdot \mathbf{B} = 0$ condition whenever the magnetic field vector was more than 20° from the satellite's spin plane. The normal sampling rate was 32 s^{-1}, and the $-\mathbf{v} \times \mathbf{B}$ electric field owing to the satellite's orbital motion has been removed. Because of a loss of contact to a guard electrode on one of the spherical sensors a few months into the mission, that axis became sensitive to density variations. Since most electron injections after onset result in rapid changes in the density and temperature of the plasma sheet electrons, we have opted not to use the spherical sensor data here. Spin-averaged measurements from the cylindrical sensors using a least squares fit to a sine wave over one spacecraft rotation are the primary data source for this analysis. Since new information for both components is available twice per spin period, we use sliding least square fits to one spin cycle of data to provide 15-s averages of the electric and magnetic fields. This restricts our derived wave-power vectors to frequencies below 34 mHz. During the discovery event of CRRES orbit 540, which led to the present study, the spherical sensors worked as intended because of slow variations in density. At the highest time resolution, measurements from the spherical and cylindrical probes agreed. *Maynard et al.* [1996b] established that the major power propagating along the magnetic field and associated with onsets occurred within or close to the Pi2 frequency band, making higher resolution unnecessary.

We analyzed in situ measurements of the Poynting vectors, $\delta\mathbf{S} = \delta\mathbf{E} \times \delta\mathbf{B}/\mu_o$, for low-frequency electromagnetic waves detected prior to and during substorm onsets and expansions. Here $\delta\mathbf{E} = \mathbf{E} - \mathbf{E}_o$ and $\delta\mathbf{B} = \mathbf{B} - \mathbf{B}_o$, where $\mathbf{E}_o$ and $\mathbf{B}_o$ are the background electric and magnetic fields. We refer to $\delta\mathbf{S}$ as the wave-power vector to distinguish it from the total Poynting vector, $\mathbf{S} = \mathbf{E} \times \mathbf{B}/\mu_o$, which includes the background electromagnetic energy transport.

Electric and magnetic field measurements are displayed in units of mV/m and nT, in VDH coordinates. $\hat{\mathbf{H}}$ is antiparallel to Earth's dipole. $\hat{\mathbf{D}}$ points toward the east. $\hat{\mathbf{V}}$ completes the right-hand system pointing almost radially outward. VDH coordinates are preferred for displaying field data because the CRRES apogee was within the nominal hinging distance and where

the cross-tail current wraps around the inner magnetosphere. For clarity, much of the orbital variation of the magnetic field is removed by subtracting the International Geomagnetic Reference Field (IGRF) model from CRRES magnetic field measurements. The measurements are displayed as $\Delta\mathbf{B} = \mathbf{B} - \mathbf{B_{IGRF}}$. The IGRF model is also used to estimate CRRES's ground track. We note, however, that the near-geosynchronous magnetic field is usually stretched with respect to dipole, and the IGRF model thus places CRRES footprints poleward of their actual positions.

The period of interest extends from December 1990 through March 1991, when the apogee of CRRES was in the late-evening and midnight sectors. Satellite measurements are supplemented with ground magnetometer data acquired from a variety of sources including the Canadian Auroral Network for the OPEN Program Unified Study (CANOPUS), the International Monitor for Auroral Geomagnetic Effects (IMAGE), the UK Sub-Auroral Magnetometer Network (SAMNET), the Solar-Terrestrial Energy Program (STEP) Project 6.4, and selected Russian stations. Occasionally, because some ground magnetometer data are hard to obtain, the times of ground onsets are determined from the *AL* index, a preliminary version of which was especially prepared for the CRRES substorm study interval (A. Yahnin, private communication, 1995).

3. Preview and Definitions

Events surrounding onsets are complex. Yet within this complexity, there are reliably repeated signatures. In the minutes prior to and including local onset at CRRES, electromagnetic signatures were consistent from one event to another. Some of these electromagnetic signatures are seen here for the first time and within the new context of derived wave-power vectors. Before presenting the observations, we preview these signatures and provide needed definitions.

Figure 2 provides a template for comprehending CRRES observations surrounding substorm onsets. The figure represents about a 30-min interval in which idealized plots are shown of the X magnetic component observed at the auroral station registering substorm onset and $S_{\|}$, E_D, and B_H observed at the magnetically conjugate location of CRRES in the inner plasma sheet. Ground onset occurs when the substorm electrojet appears as evidenced by the start of an X-component bay at a ground magnetometer station conjugate to CRRES. Local onset at CRRES is defined by the earlier of (1) the start of dipolarization and coincident appearance of the SCW or (2) the start of the explosive increase of the power ($S_{\|}$) flowing toward the ionosphere. The second choice is called local explosive onset (LEXO). As this is presumably the power responsible for the substorm surge, LEXO is an obvious definition for local onset. However, in most events, dipolarization begins gradually, along with an accompanying SCW, before LEXO. To be consistent with the definition of ground onset, in those cases, local onset is defined as the start of dipolarization. There are seven consistent signatures associated with substorm onsets observed at CRRES enumerated in Figure 2 which we describe below. This key is used throughout the rest of this paper.

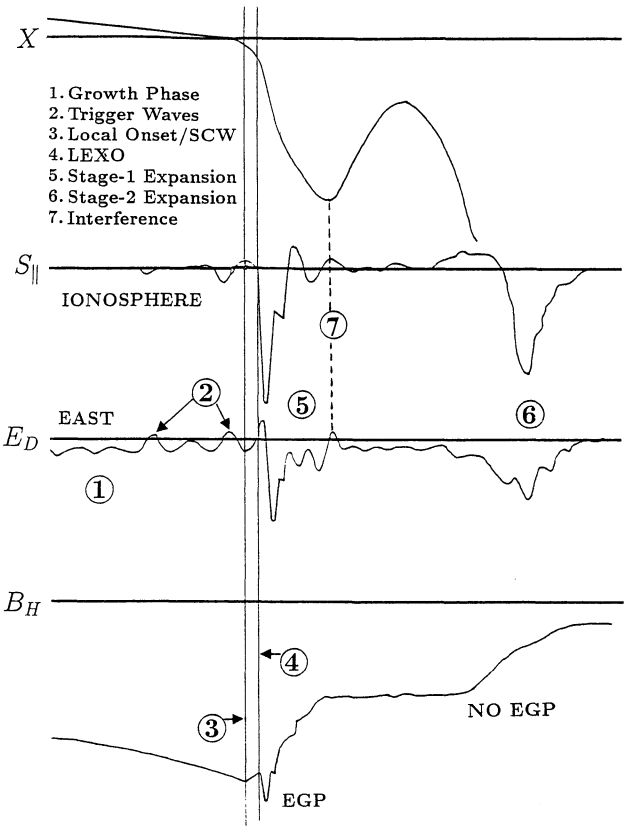

Figure 2. An illustration representing CRRES observations surrounding substorm onsets. The top plot shows the ground X magnetic component. The remaining three plots show $S_{\|}$, E_D, and B_H. Recurring features of the observations are enumerated.

3.1. Growth Phase (Step 1)

Prior to local onset a substorm growth phase is evidenced at CRRES by a stretching of the magnetic field. In addition, as CRRES enters the plasma sheet from the plasmasphere, a small, net westward electric field is usually evident. A most emphatic exhibition of the growth phase is discussed by M96 (orbit 540). Generally, the persistence of region-2 FACs and the Harang discontinuity (HD) indicate the presence of background earthward convection [*Erickson et al.*, 1991]. Such background convection prior to substorm onset, if not a convection bay, corresponds to a growth phase [*Erickson and Wolf*, 1980; *Hau et al.*, 1989]. Of particular importance during the growth phase are oscillations of the electric field with 60- to 90-s periods impressed on the background, westward electric field. Pi2 band waves are associated with establishment of the SCW at onset.

3.2. Trigger Waves (Step 2)

The amplitudes of electric field oscillations increase from time to time, causing eastward excursions of the total electric field. When the electric field turns eastward, $\mathbf{j} \cdot \mathbf{E} < 0$, the drift wave couples to the Alfvén mode (ballooning), and plasma kinetic energy is converted into electromagnetic energy, which flows toward the ionosphere. Lesser power flows away from the ionosphere as the electric field becomes westward again. We assume the latter is power reflected from the ionosphere that was originally released toward the ionosphere when the electric field was eastward. The first low-frequency wave power, usually observed coincident with an eastward excursion of the electric field, flows mainly toward the ionosphere with a much smaller component perpendicular to $\mathbf{B}_o$. The onset process begins with such eastward excursions of the electric field. Hence we call these trigger waves. One or more such trigger waves occur prior to the start of substorm expansion. The last of these preceding expansion is the LEXO.

3.3. Dipolarization Begins and the SCW Appears (Step 3)

When energy is released from the plasma during eastward electric field excursions faster than the background convection energizes it, cross-tail drift current is reduced, dipolarization starts, and the SCW forms. This usually occurs at or before ground onset and LEXO. Thus, according to the definition provided above, the start of dipolarization usually marks local onset. Associated with this stage, 30-s-period oscillations of $\mathbf{B}$ appear. (This is not clear in the 15-s data presented here, but it is obvious in the 5-s data.) The electric field continues oscillating with periods of 60 to 90 s.

3.4. Local Explosive Onset (Step 4)

Except when LEXO occurs first, within two periods of the electric field oscillation after dipolarization begins, an explosive increase in the energy flowing toward the ionosphere (LEXO) occurs as the electric field becomes eastward again. This is the start of a monotonic increase to peak power delivered locally to the ionosphere. The power peaks at substorm surge levels sometime during the interval from peak eastward electric field and peak westward electric field a half cycle later (the start of the expansion, step 5 below). This explosive release of energy toward the ionosphere often precedes our best determination of ground onset. Significant magnetic field compression, large transient FACs, and EGP signatures are observed in association with LEXO and the start of substorm expansion.

3.5. Stage-1 Expansion (Step 5)

One half a wave cycle after the explosive energy release begins, the electric field turns westward and is enhanced over its growth-phase values. This marks the start of the expansion phase. Power flowing toward the ionosphere, which started while $\partial E_D/\partial t$ was eastward in step 4, usually continues to increase as the electric field turns westward. The rate of dipolarization usually increases following the start of expansion. Electron injection accompanies this dipolarization following the start of expansion. The drift-wave, Pi2 oscillations of the electric field continue but with shorter periods.

The FACs of steps 4 and 5 are complicated mixtures of the SCW and FACs of the energy-release waves. The observed electromagnetic oscillations are consistent with oblique Alfvén waves traveling toward and away from the ionosphere. Up to step 4, power toward the ionosphere is associated with eastward electric fields. Transient FACs associated with this wave are upward on the dawnside and downward on the duskside of the wave, opposite to the sense of the SCW. Reflected power is associated with westward electric fields. Since $\mathbf{j} \cdot \mathbf{E} < 0$ during times when power flows toward the ionosphere, we assume that power originated locally from conversion of plasma kinetic energy into electromagnetic energy. Following start of the expansion phase, the electric field is westward while $S_\parallel$ is toward the ionosphere. The downward wave FACs are now of SCW sense. Conservation of energy requires the introduction of power from a nonlocal source. The trigger and onset waves also persist into the expansion. They appear to have azimuthally aligned planar fronts and to propogate toward the west.

3.6. Stage-2 Expansion (Step 6)

The initial expansion at CRRES is usually short-lived ($\leq$10 min). During this interval, drift-ballooning waves, like those observed by *Roux et al.* [1991], pass by the satellite with decreasing amplitudes. We refer to the initial expansion, which was immediately preceded by LEXO and includes EGP signatures and a significant wave δB, as a stage-1 expansion. Often, within $\sim$10 min after stage-1 expansion activity diminishes at CRRES, westward electric field increases again, accompanied by significant wave power flowing toward the ionosphere. Electrojet intensification is coincident with this new stage of expansion. We call this intensification stage-2 expansion. Unlike stage-1 expansions, which are initiated by LEXOs and eastward electric fields, the second (and later stages) of expansions appear in the near-geosynchronous region as enhancements of westward electric field and do not have a LEXO, EGP signatures, or significant wave δB even though Pi2 oscillations are superposed.

3.7. Interference (Step 7)

Often, after the start of the initial expansion, the electric field can turn eastward again. If this occurs while power is flowing away from the ionosphere, the electrojet wanes or can turn off completely. Some portion of expansion power flowing toward the ionosphere with westward electric field reflects and changes phase

by 180°, i.e., reflected power has eastward electric field. The drift waves that led to onset persist during expansion. Hence interference should not be surprising and is apparent in about half of the events. Sometimes interference is minor and is soon overwhelmed by a stage-2 expansion. When the expansion is weak and stage 2 is delayed, the interference can shut off the expansion until another LEXO and stage-1 expansion initiate.

4. Observations

We have examined more than 400 possible substorm events while CRRES was near apogee in the nightside plasma sheet between December 1990 and March 1991. The events were identified either by variations of the *AL* index or substorm-like activity in magnetic fields observed by CRRES. Of these, the 20 events listed in Table 1 occurred while (1) CRRES was within the magnetic local time (MLT) sector of a substorm onset, (2) good electric and magnetic field measurements were obtained, and (3) the third component of the electric field could be computed using the $\mathbf{E} \cdot \mathbf{B} = 0$ condition. This last criterion required that CRRES be situated away from the magnetic equator. The 20 events included isolated onsets, multiple onsets, and two pseudobreakups. A like number of local onsets that were just west or east of the onset sector were also found. The remaining events were rejected because signatures were too weak, CRRES was located too far west/east of the SCW at onset, or the overall levels of geomagnetic activity were too high to permit identification of either local substorm onset or CRRES's position with respect to the SCW.

Dipolarization is evidenced by a decrease in $|\Delta B_V|$ and/or an increase in ΔB_H, usually accompanied by a change in the trend of $|\Delta \mathbf{B}|$. As CRRES was removed from the magnetic equator for this study, evidence of FACs appears in variations of the magnetic *D* component. Proximity to onset's central meridian occurred when CRRES was situated within the MLT sector across which the SCW formed and is confirmed by the lack of evidence of an approaching leg of the SCW. Onset characteristics observed within the MLT sector of the forming SCW had a sharpness that was lacking when CRRES was initially outside of it. If CRRES was east of the onset sector, signatures of local expansion onset were usually not sharp and clear. If CRRES was west of the onset sector, the rate of magnetic field stretching gradually increased as the upward leg of the SCW approached the spacecraft, the *D* magnetic perturbation grew gradually and decreased symmetrically, and the peak perturbation of the *D* component coincided with the change from enhanced stretching to dipolarization.

The events in Table 1 were selected because expansion phase onset was sharp in the absence of evidence of an approaching leg of the SCW. Events P and S do show some SCW perturbation of the magnetic *D* component just before local onset. However, the signatures of the onsets were so consistent with other events observed within an onset sector that we regard events P and S as being initially at the western edge of the onset sector. Events C, M, P, R, and S display dual-onset signatures, in which a pair of LEXO waves passed over CRRES.

Once events in Table 1 were identified, ground data were searched for onsets, and the earliest ground onset times were estimated from magnetometer traces and/or *AL*. M96 discuss how the Harang discontinuity (HD) can be used to establish the relative position of CRRES with respect to its field-line mapping to conjugate ground stations, both prior to onset and as the SCW expands. The *V* and *H* components of the electric field reveal if the satellite is east or west of the HD. On the ground, the magnetic *X* component reveals if a station is in the eastward (west of the HD) or westward (east of the HD) electrojet region. In none of the 20 events, when conjugate ground data were available, did we find any inconsistency with our contention that CRRES was situated within the local-time sector of the SCW at onset.

M96 discussed events D and E (orbit 540) at length and computed the component of $\delta\mathbf{S}$ along, but not its components perpendicular to, $\mathbf{B}_o$. Event E was our discovery event and is of particular interest because the onset was isolated, occurring after 6 hours of quiescence, and localized over Dixon. CRRES was in good magnetic conjunction with Dixon, within the upward leg of the SCW as it formed, and within the inner edges of the electron plasma sheet. The observed field and particle behavior associated with this onset is presented in detail by M96 and is not repeated here. Below, we provide specific analyses of events A and P. Event A is one of the more simple onsets which exhibits all seven signatures previewed above most clearly. Event P is an example of a dual onset and also clearly illustrates interference (step 7), a delayed stage-2 expansion (step 6), and an example of an isolated earthward flow burst (EFB). As we discuss later, an EFB is likely the near-geosynchronous remnant of a high-speed flow spawned during a stage-2 expansion or recovery phase.

4.1. Event A, Orbit 461

At 0841.5 UT on January 31, 1991, while CRRES was inbound from apogee near ~0040 MLT it encountered an onset. This event was rather weak on the ground, but we choose to display this event because the different steps of onset and expansion (see Figure 2) are separated and clearly identifiable. Figure 3 shows the CRRES ground track in relation to the CANOPUS magnetometer chain from 0815 to 0915 UT. At onset, CRRES mapped to the east and south of Fort McMurray (MCM). Figures 4a, 4b, and 4c show the *X*, *Y*, and *Z* magnetic components from (top to bottom) Fort Churchill (CHU), Back (BAC), Gillam (GIL), MCM, and Fort Smith (SMI). There are no data from Rabbit Lake (RAB) for this particular event. Vertical lines de-

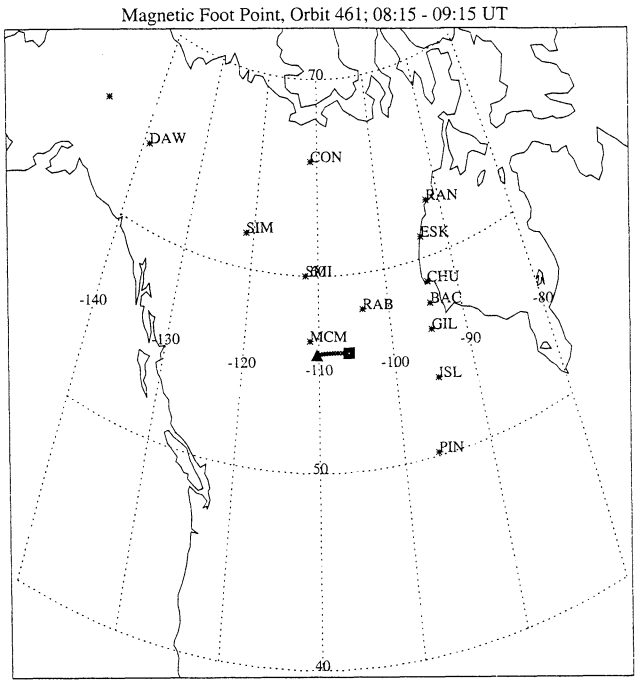

Figure 3. Event A. CRRES ground track from 0815 to 0915 UT on January 31, 1991 over the CANOPUS magnetometer network.

note ground onset and the onset of activity poleward. Ground onset was recorded at MCM and GIL at 0845.6 UT. Plate 1 shows 6300-Å and 5577-Å auroral emissions observed by the Gillam meridional scanning photometer. Prior to onset, MCM and GIL were on opposite sides of the HD, as evidenced by the different variations of the X components.

Onset was closer to MCM than to GIL. At MCM the Z component turned positive after onset, indicating that the westward electrojet was located to the south as it intensified. The electrojet initially intensified south of GIL. The negative Y component at MCM and SMI is consistent with the SCW being eastward of the stations [*Orr and Cramoysan*, 1994]. At ~0852 UT, activity began to grow at BAC and CHU, while activity diminished to the south. Almost simultaneously a band of auroral emissions observed by the Gillam meridian scanning photometer progressed poleward. After 0905 UT, the event was over at CRRES, and activity became weak and complex on the ground. Optics showed a split auroral zone with weak activity. At no time was there rapid poleward expansion of the poleward boundary, which would be indicative of a NEXL reconnecting lobe flux [*Maynard et al.*, 1997].

Starting at 0830 UT the scanning photometer at Gillam detected that ground onset was preceded by

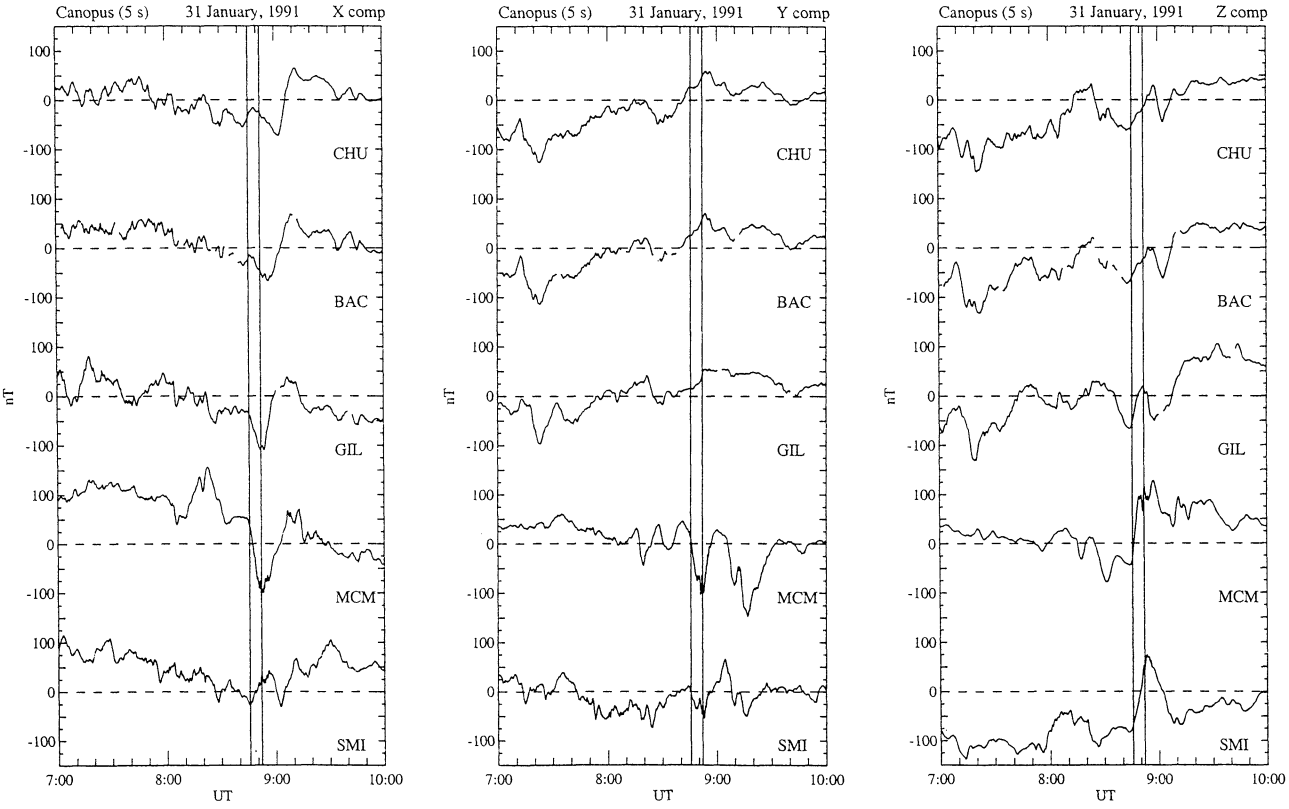

Figure 4. The (a) X, (b) Y, and (c) Z magnetic components observed at selected CANOPUS stations from 0700 to 1000 UT on January 31, 1991.

an intensification near the poleward auroral boundary [*Lyons et al.*, 1999]. We interpret this intensification at the poleward border as reflecting increased reconnection at the distant X line [*Maynard et al.*, 1997]. No optical or magnetic evidence connects this intensification with the onset region near 64° prior to onset. As we turn our attention to CRRES observations, two features of the ground measurements should be kept in mind: (1) the intensification of the equatorward arc and magnetic bay at 0845.6 UT, and (2) the poleward progressing auroral emissions and electrojet starting at ~0852 UT.

Figure 5 shows the components of **E** and $\Delta\mathbf{B}$ in VDH coordinates and $|\Delta\mathbf{B}|$. Figure 6 shows the wave-power vector $\delta\mathbf{S}$ in VDB coordinates, including $S_{\parallel}$ on an expanded scale, and E_D for the same interval. The seven key, electromagnetic features associated with onsets and expansions in the near-geosynchronous region previewed above are pointed out in Figures 5 and 6. Vertical lines mark local onset (step 3) and the start of the explosive energy release (LEXO, step 4) at CRRES. Electron injection to the CRRES orbit is indicated by the pi symbol.

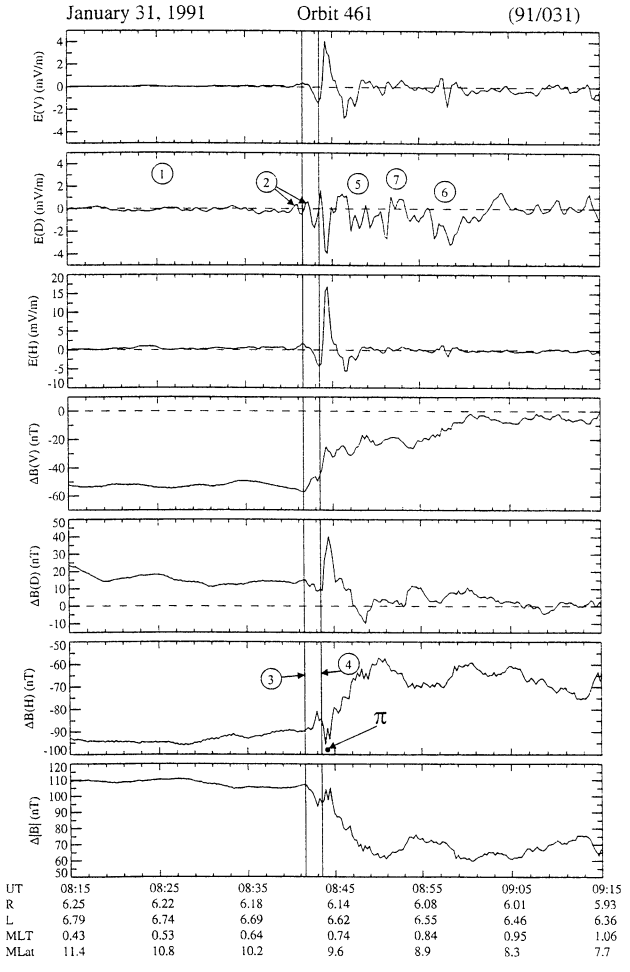

Figure 5. Event A. CRRES electric and magnetic field measurements from 0815 to 0915 UT during orbit 461 on January 31, 1991.

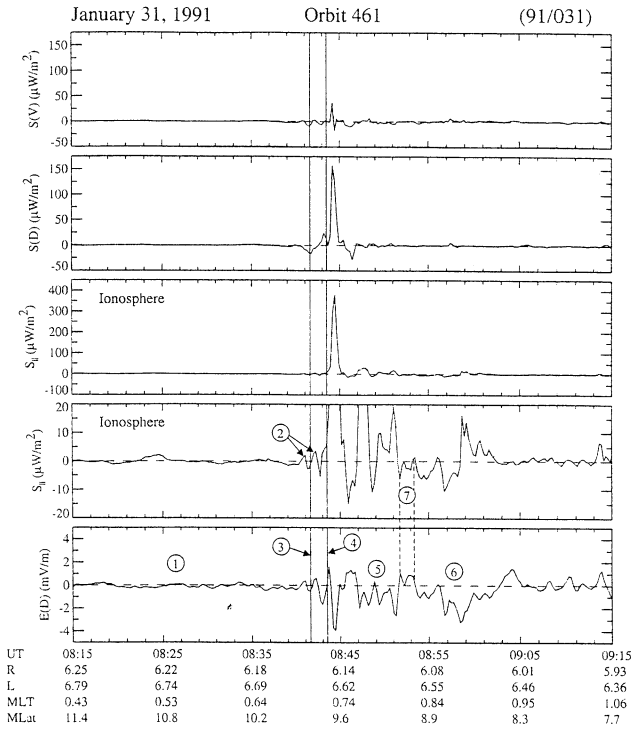

Figure 6. Event A. Three components of the wave-power vector $\delta\mathbf{S}$ derived from CRRES electric and magnetic field measurements, $S_{\parallel}$ on expanded vertical scale, and E_D from 0815 to 0915 UT during orbit 461 on January 31, 1991.

The weakly positive E_V and E_H observed during the growth phase (Figure 5) map to the ionosphere as poleward electric fields, indicating that CRRES was west of the HD. The background, positive ΔB_D deflection results from downward region-2 FAC earthward of the satellite. There are two trigger waves (step 2) prior to local explosive onset. The electric field oscillations resulting in the trigger waves and LEXO are particularly regular in the present example.

Between the time when the SCW appeared (left vertical line) and the explosive increase in the power delivered to the ionosphere began (right vertical line), the meridional electric field reversed direction, indicating the satellite moved east of the HD. This is consistent with our contention that CRRES was within the SCW as it formed. The reduction of ΔB_D indicates that the satellite is nearer the upward leg of the SCW located earthward of the satellite. Alternatively, the satellite could be nearer the downward leg of the SCW, which would be located tailward of the satellite. However, as the SCW develops, the wave-power vector gains an eastward component. Our experience indicates that the larger power is associated with the upward (duskside) leg of the SCW. This is evidenced in the ionosphere by the WTS. Thus we prefer the first alternative: The satellite is nearer the upward leg of the SCW whose centroid is located to the west and earthward of the

satellite. This interpretation is consistent with the conjugate ground observations.

Note that dipolarization starts at 0841.5 UT following the first trigger wave, 4 min before ground onset. LEXO occurs at 0843.4 UT, over 2 min before ground onset. The peak power is observed at 0844.5 UT, 1 min prior to ground onset. As seen in Figure 6, at LEXO the power delivered to the ionosphere begins an explosive increase toward its peak level. In the present example the measured peak power of 370 μW/m^2 projects to 200 mW/m^2 when mapped to the ionosphere and occurs at peak westward electric field. (Power mapping to the ionosphere is approximated by multiplying the measured parallel power by 55,000 nT/$|\mathbf{B}|$.) The meridional component of the $\mathbf{E} \times \mathbf{B}$ drift velocity spikes at ~40 km/s earthward at this time. At first glance, this flow speed does not seem very large. However, it must be remembered that our observations are being made significantly away from the magnetic equator. Growth phase flows are typically ~5 km/s at this observation point. The tailward meridional flow associated with the eastward electric field during LEXO is 13 km/s in the present example.

At LEXO an EGP signature occurs. A magnetic compression is evident during the oscillation cycle that begins at LEXO and includes the peak, westward expansion electric field. In the present example, $\delta B/B$ reaches 0.114. While the negative deflection of the background magnetic D component most likely still results from the upward leg of the SCW earthward of the satellite, the transient, positive D deflection associated with the surge-sized power flowing toward the ionosphere results from the FACs associated with the LEXO/expansion wave. At LEXO the EGP depression of ΔB_H occurs while $\partial E_D/\partial t$ is eastward. This indicates that the wave is mainly earthward of the satellite. Thus the positive D magnetic deflection indicates proximity to a downward FAC filament. The positive D magnetic deflection does not actually start until $\partial E_D/\partial t$ becomes westward. At this time the EGP depression recovers, while power is still increasing toward the ionosphere. Electron injection (π) occurred at this time. The LEXO wave has given way to an expansion wave carrying FACs of SCW sense. The positive D magnetic deflection thus indicates proximity to the eastward portion of the wave. This is consistent with the eastward component of the wave-power vector observed at this time. The transient D magnetic deflection disappears, and the enhanced westward electric field ends by 0845 UT as the expansion wave drifts to the west. However, 2 min later, one sees a similar, but much weaker expansion wave approaching from the east. The wave-power vector has a westward component immediately preceding its arrival. As it arrives, the magnetic D deflection is negative, consistent with upward current on the western side of the second, weaker expansion wave. Periodic waves continue to drift by CRRES during the expansion, but with much less power [c. f. *Roux et al.*, 1991].

At ~0852 UT there was interference (step 7), and the first stage of the expansion at CRRES ended. However, at 0853.5 UT a second stage expansion (step 6)

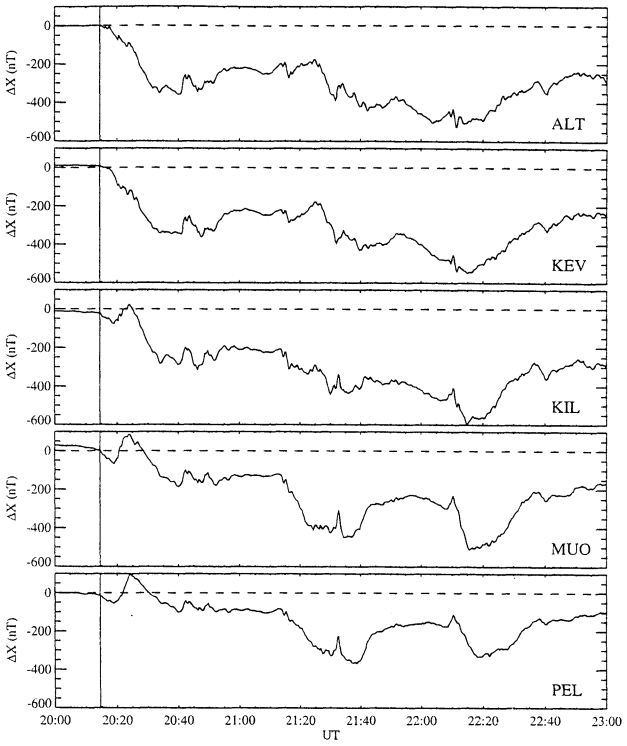

Figure 8. The X magnetic component observed at the IMAGE stations from 2000 to 2300 UT on March 17, 1991.

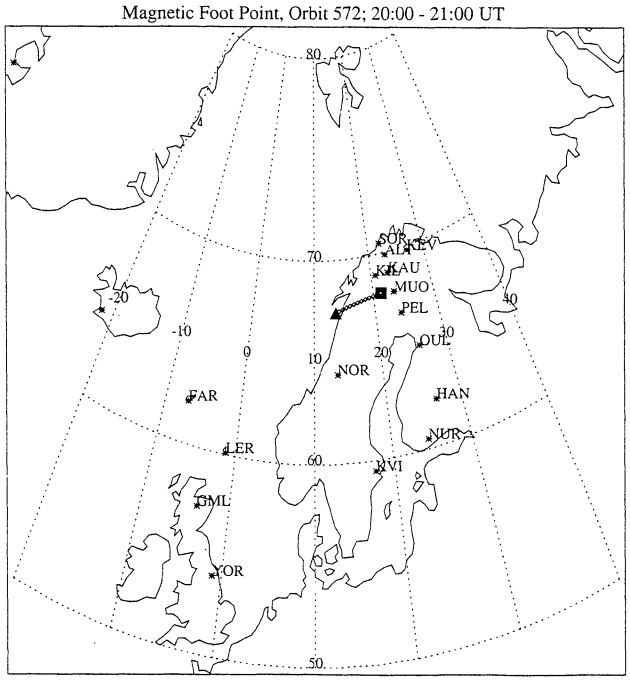

Figure 7. Event P. CRRES ground tracks from 2000 to 2100 UT during orbit 572 on March 17, 1991.

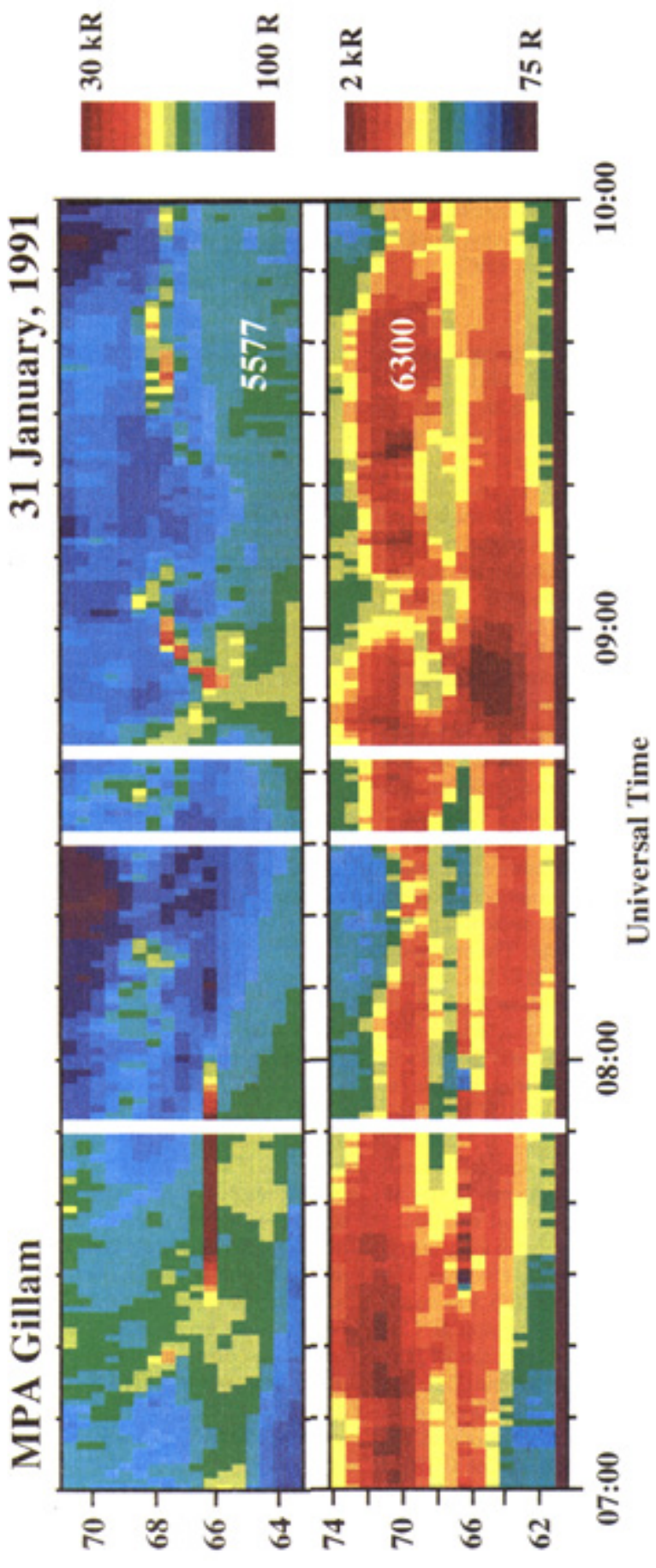

Plate 1. The 6300-Å and 5577-Å emissions from the Gillam scanning photometer from 0700 to 1000 UT on January 31, 1991.

began, albeit very weakly, roughly in correspondence to the poleward progressing band of auroral emission observed at Gillam. Notice that the stage-2 expansion looks like neither the earlier onset nor the second expansion wave following onset. There were no LEXO or EGP signatures nor was there a major magnetic compression. When compared with the ground optics, a NEXL may have formed at this time at which reconnection progressed toward lobe field lines, but the process stopped before engaging the lobe [*Maynard et al.*, 1997].

4.2. Event P, Orbit 572

Event P was the first of three onsets during a 2-hour interval over Scandinavia on March 17, 1991. Observations from these event were described in detail by *Yeoman et al.* [1994]. Event P had a dual onset, with interference between onsets. Also, about 27 min after the initial onset, CRRES data show an isolated EFB.

Figure 7 shows that the CRRES ground track from 2000 to 2100 UT on this day mapped slightly to the west and north of the IMAGE magnetometer station Muonio (MUO) and moving to the northwest. Figure 8 shows the X magnetic component at the IMAGE stations from 2000 to 2300 UT. At 2014.5 UT a bay commenced at all stations. Pi2 onsets occurred at midlatitude stations at about 2016 UT [*Yeoman et al.*, 1994]. Pi2 onsets were recorded over the SAMNET stations at 2014.5 and 2031.5 UT. The Z-component traces (not shown) indicate that the substorm electrojet is between Pello (PEL) and MUO. At 2018.5 UT the X component recovered at the lower-latitude stations only to reintensify at 2024.5 UT. At 2021 UT, Oulu shows a Pi2 intensification at the same time as the Z component traces at all IMAGE stations turn negative, indicating that the electrojet moved north of the chain. The westward electrojet remained to the north until 2112 UT, when a new onset occurred near the lower-latitude stations.

The key ground times are (1) onset at 2014.5 UT, (2) low-latitude recovery at 2018.5 UT, and (3) the Pi2 intensification at 2021 UT at Oulu associated with resumption of the low-latitude bay over IMAGE at 2024.5 UT.

Figure 9 shows the components of $\mathbf{E}$ and $\Delta\mathbf{B}$ as well as $|\Delta\mathbf{B}|$ during this first substorm interval. Early in the interval (step 1), the electric field had earthward and northward components. Mapped to the ionosphere, these indicate that CRRES was east of, but near, the HD prior to the start of activity. CRRES was again east of the HD after the end of the expansion at CRRES's location at 2028–2030 UT until after the EFB at 2043.5 UT (dashed vertical line). MUO and PEL are in the positive bay region, i.e., west of the HD based on magnetometer records, prior to onset. Stations to the north were in the negative bay region. Since CRRES mapped to the north and west of MUO near the time of onset, CRRES was probably near the electric field reversal of the HD. Figure 10 shows $\delta\mathbf{S}$ and E_D during the interval.

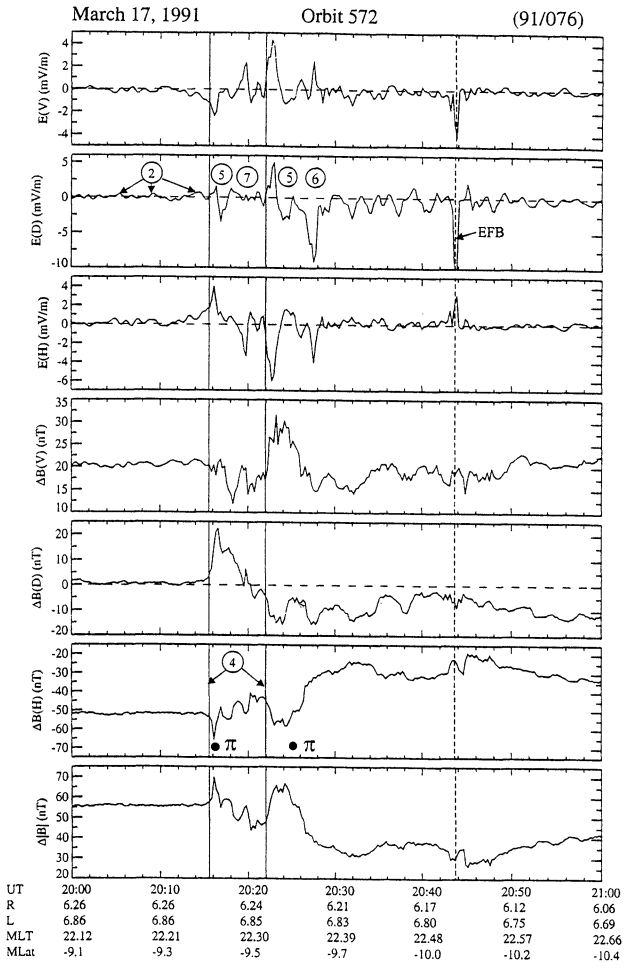

Figure 9. Event P. CRRES electric and magnetic field measurements from 2000 to 2100 UT during orbit 572 on 17 March 1991. The dashed vertical line denotes an earthward flow burst (EFB).

At CRRES, onset appears to proceed in two steps preceded by three weak, but growing trigger waves (step 2) at 2006.1, 2009.4, and 2013.5 UT. A sharp onset (LEXO) is observed at 2015.4 UT (step 4) with an accompanying EGP, field compression, and the appearance of a FAC (ΔB_D). This occurred 1 min after ground onset, followed shortly by an expansion start (step 5) which appeared to be rather weak. Dipolarization stopped completely near 2020 UT. The wave power was out of phase with E_D between 2018.4 and 2022 UT, indicating interference (step 7). This occurred as the X-component recovery began at IMAGE. The signals returned to being in phase at 2022 UT when a second LEXO was seen at CRRES, about 1 min after the Pi2 onset over Oulu and 2.5 min before the reintensification over IMAGE. The EGP signature as well as the eastward spike in E_D appear to last longer than usual, but all the repeatable signatures of LEXO (step 4) are present. Following the second LEXO, dipolarization resumed, and a second expansion (step 5) began at 2023.4 UT, associated with reflected power arriving from the

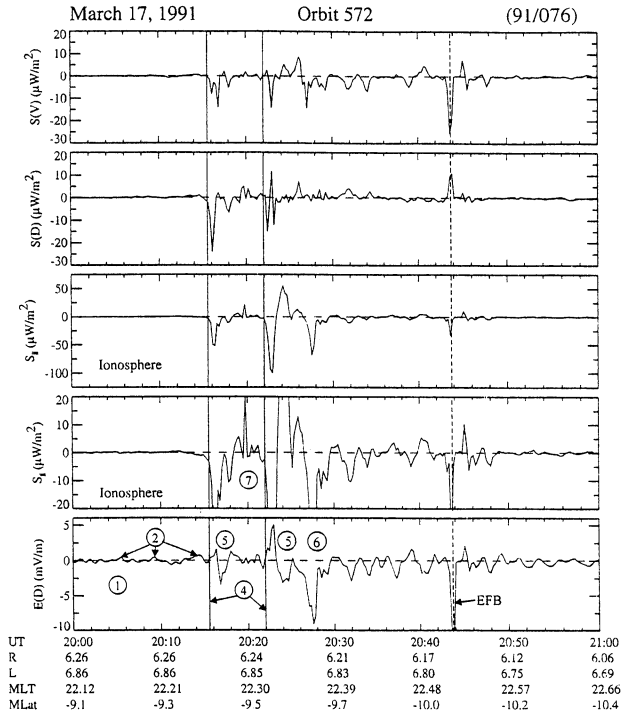

Figure 10. Event P. Three components of the wave-power vector $\delta\mathbf{S}$ derived from CRRES electric and magnetic field measurements and E_D from 2000 to 2100 UT during orbit 572 on March 17, 1991.

ionosphere. The rate of dipolarization slowed just as E_D and $S_{||}$ vanished for an instant at 2025.2 UT. At this point, E_D and $S_{||}$ have the signatures of a stage-2 expansion start (step 6), possibly triggered by the first LEXO. The electric field became westward again in association with power arriving from the ionosphere. The westward electric field continued to intensify as wave power became downward toward the ionosphere and intensified. The expansion-phase westward electric field peaked at 2027.8 UT. At this time, meridional E/B spiked at 75 km/s earthward.

Note that prior to the dual onsets CRRES was to the east of but near the HD. After the onsets, CRRES was clearly east of the HD. The region-2 FAC is upward east of the HD, which in the southern hemisphere causes a positive deflection of the magnetic D component. The small positive deflection seen prior to the first onset attests to the proximity of CRRES to the HD at this time. The EGPs associated with the dual onsets indicate that the wave source was primarily earthward of CRRES. Thus the increase of the magnetic D component following local onset (step 4) indicates an upward FAC. As the event at CRRES occurred approximately 1 min after and to the west of ground onset, this is consistent with the upward leg of the SCW and is verified by the westward component of the wave power following local onset. Spiky features superposed on the D deflection result from the waves. As the westward side of the LEXO wave has downward FAC, we expect to observe a negative deflection of the D magnetic component as the second onset wave arrives earthward of CRRES, and this is what is seen. Following the second onset wave, CRRES was in the downward leg of the SCW, and, following the stage-2 expansion signatures, the wave Poynting flux becomes weak and nondescript. Unlike the upward leg of the SCW, which is sharp and concentrated, the downward leg becomes rather diffuse. The same diffuse nature of the downward leg of the SCW was reported by *Maynard et al.* [1998a] surrounding observations during CRRES orbit 491.

We call attention to the EFB seen in Figures 9 and 10 at 2043.5 UT (dashed vertical lines). The signatures of this flow burst are typical of others seen in the data. The bursts we have found occurred well after onset of an expansion at CRRES. As one would expect, the signatures are of an enhanced westward electric field, modest compression of the magnetic field (seen in ΔB_H and confirmed in $|\Delta\mathbf{B}|$), and wave power toward the ionosphere. EFBs were not observed preceding substorm onsets and SCW formation. Rather, they look like short stage-2 expansions or near-geosynchronous remnants of bursty bulk flows.

4.3. Event Statistics

Figure 11 shows the L versus MLT locations of CRRES at the 18 expansion onsets (pseudobreakups were excluded). The average MLT of the 18 onsets is 2241 MLT, with a standard deviation of 50 min. Table 2 lists the relevant timing surrounding the 20 events. The nine columns provide (1) event designations, (2) CRRES orbit numbers, (3) ground onset times, (4) sizes of the magnetic bays, (5) times of the first trigger waves, (6) times of local onsets, (7) times of LEXOs, (8) times of the starts of expansions, and (9) injection times. Table 3 provides timing statistics for key steps in substorm development observed at CRRES. The first column lists the observation while the last column provides the time of its occurrence relative to ground onset. The middle column lists the time separation between the steps.

The first trigger waves were observed at CRRES, on average, 5.5 ± 3.1 min prior to ground onset. Dur-

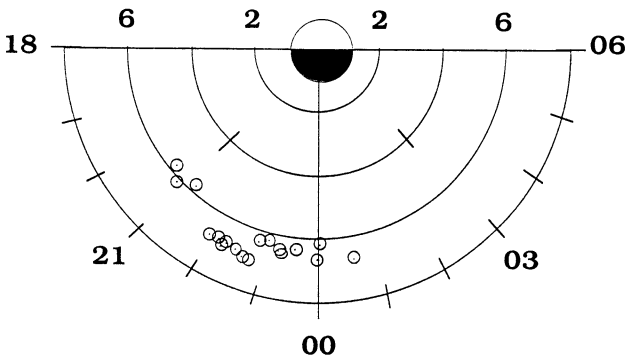

Figure 11. Position of CRRES, L versus MLT, just prior to the local expansion onsets listed in Table 1.

Table 2. Substorm Timing at CRRES

Event	Orbit	Ground Onset	Bay, nT	First Trigger Step 2	Onset[a] Step 3,4	LEXO Step 4	Expansion[b] Step 5,6	Injection
A	461	0845.6	150	0840.0	0841.5	0843.4	0843.8	0844
	stage 2	0852					0853.6	
B	481	1302		1259.5	1300.5	1304.6	1305.5	1303.5
	stage 2	1318	480			1318.5	1318.7	1319.3
C_α	484[c,d]	1653		1639.7	1658.9	1658.9	1659.2	1659.5
C_β		1703.5	540		1702.3	1702.3	1703.3	
D	540[e]		25	1917.2	1918.3	1922.8	none	
E	540	1938	550	1937.8	1938.5	1940.7	1941.9	1942.5
F	545[e]	1941.3	115	1933.6	1936.4	none	none	
G	545	1952.3	250	1944.1	1952.3	1952.3	1954.2	
	stage 2	1957	885				1956.9	
H	545	2018	730	2016.6	2016.6	2017.6	2018.5	2018,2020.5
	stage 2	2034.8	440				2035.7	2038
I	546[g]	0321	130[h]	0316.9	0320.1	0321.0	0324.1	0324
	stage 2	0333	210[h]				0331.0	0331
J	547	1320		1315.7	1321.4	1324.5	1325.6	1326
	stage 2	1330					1330.8	1331.5
K	547	1412	250[h]	1407.3	1407.8	1411.3	1411.7	NA[i]
L	547	1436	535[h]	1429.3	1439.3	1440.6	1442.7	NA
M_α	550[c]	2112	445	2104.6	2110.0	2110.7	2110.9	2112
M_β		2120	750		2118.8	2120.3	2120.9	
N	552	1317	220	1303.4	1315.8	1317.2	1317.7	NA
	stage 2[f]	1328	550				1341.1	
O	553	NA	125[h]	0116.8	0121.9	0124.2	0124.5	0123,0124,0125
	stage 2	0200[j]	400[h]				0147.4	
P_α	572[c,g]	2014.5	50	2006.1	2015.4	2015.4	2016.5	2016[k]
P_β		2021	325		2022.0	2022.0	2023.4	
	stage 2						2025.2	2025[k]
Q	577	2258	195	2255.6	2257.0	2257.9	2258.2	NA
	stage 2	2311.5	700				2312.5	
R_α	583[c]	0825	340	0825.0	0826.6	0830.4	0831.0	0830
R_β			430		0832.2	0832.2	0833.5	
S_α	586[c,g]	1126	275[h]	1123.0	1125.1	1128.5	1129.1	1129
S_β					1130.6	1130.6	1132.2	
	stage 2	1145					1145.5	1146
T	593[l]	0847	520	0840.8	0844.7	none	0847.6	0847.5

[a]Earlier of the start of dipolarization and local exploxive onset (LEXO).
[b]Time when expansion electric field begins.
[c]Dual onset.
[d]Previous onset at 1630 UT.
[e]Pseudobreakup.
[f]Initially outside of substorm current wedge during stage-2 expansion.
[g]At the western edge of onset sector.
[h]Determined from *AL*.
[i]Data not available.
[j]Late at Leirvoguir.
[k]From Figure 5 of *Yeoman et al.* [1994].
[l]Storm time.

ing events C and N, the first trigger wave was observed more than 13 min prior to ground onset. The pseudobreakups, events D and F, began 20 and 11 min prior to events E and G, respectively. Local onsets were observed, on average, 1.1 ± 1.9 min prior to ground onset. LEXOs occurred, on average, 1.5 ± 2.2 min after ground onset. Stage-2 expansions were observed, on average, 0.4 ± 0.7 min after ground reintensifications. Reintensifications at ground and corresponding stage-2 expansions at CRRES are apparent following over half of the substorm expansion onsets.

Local onset occurred, on average, 1.9 ± 1.3 min before LEXO. (Events F and T had no LEXO phase.) LEXO marked local onset in three events, including the dual onsets C and P. In the remaining 15 events, local onset preceded LEXO by an average 2.3 ± 1.1 min.

Table 3. Near-Geosynchronous Substorm Timing Statistics

Observation at CRRES	Δt, min	Minutes From Ground Onset
First trigger wave		-5.5 ± 3.1
	4.8 ± 3.9	
Local onset		-1.1 ± 1.9
	1.9 ± 1.3	
	2.3 ± 1.1 (LEXO $\neq$ local onset)	
Local explosive onset		$+1.5 \pm 2.2$
	0.9 (0.2 to 3.1)	
Stage-1 expansion start		$+2.4 \pm 2.3$
	0.1 ± 0.8	
Particle injection		$+2.6 \pm 2.1$
(Ground reintensification)		$(+11.2 \pm 3.2)$
	(0.4 ± 0.7)	
	12.5 ± 5.3 (from stage-1 start)	
Stage-2 expansion start		$+13.7 \pm 4.8$

Interference is evident in about half the events, either occurring between dual onsets (as in event P) or associated with electrojet waning prior to stage-2 expansion (as in event A).

Table 4 provides values for the components of the wave Poynting vectors of the trigger waves immediately preceding local onsets and at peak power. The power vector components are keyed by the substorm sequence described earlier. Peak power for both stage-1 (step 4 or step 5) and stage-2 (step 6) expansions are listed. The parallel component of measured wave power is mapped to the ionosphere by multiplying the measured power by 55,000 nT divided by the local magnetic field magnitude. For reference, the average power in a typical substorm surge is estimated as 50 mW/m^2, which is the Joule heat given a typical electrojet of 1 A/m and an electric field of 50 mV/m [see *Weimer et al.*, 1994].

At the bottom of Table 4, three EFBs are listed. These are episodes of earthward plasma flows of $\sim$1 min duration. They have the expected signatures of bursty bulk flows (BBFs) [*Angelopoulos et al.*, 1992] arriving from downtail with wave power flowing toward the ionosphere, except that they do not reach 400 km/s at CRRES, having presumably slowed down considerably. Note that EFBs are not observed in association with local onsets, rather they appear after substorm expansions. They are like stage-2 expansions but turn on more sharply and have shorter duration. A few stage-2 expansions culminate in similar looking bursts. Our survey of the data set suggests that EFBs are rare at the location of CRRES.

Peak powers occurred during the LEXO phase of 10 events and at the start of the stage-1 expansion in eight events. Events F and T had no LEXO or stage-1 expansion. Power was very weak in event F, while event T represents a potential NENL-triggered expansion onset. The cases where power maximized during LEXO corresponded to maxima of the eastward electric field. Cases where the power maximized at the start of expansion usually corresponded to the first extremum of the westward electric field. However, peaks sometimes occurred just as the electric field turned westward following LEXO. Generally, wave power maximized sometime during the half-cycle between the maximum eastward LEXO electric field and the first extremum of the stage-1 westward electric field.

Table 5 contains additional statistics of the wave power during onset triggers, LEXOs, and stage-1 and stage-2 expansions (including EFBs) for the 20 events. The seven columns list (1) event stage, (2) the number of measurements in the sample, (3) the average fraction of the power contained in the parallel component, (4) the average parallel power (toward the ionosphere), (5) the maximum parallel power measured, (6) the average power mapped to the ionosphere, and (7) the maximum power mapped to the ionosphere. While values given in the second row contain only onset triggers, the values are representative of trigger waves, generally. Note that approximately 90% of the electromagnetic wave power is contained in the parallel component. Average LEXO and expansion power, when projected to the ionosphere, are typical of that seen in the WTS.

At LEXO, maximum eastward electric fields range up to 20 mV/m and are 4.8 mV/m on average. Corresponding tailward meridional flows range up to 119 km/s and are 30.6 km/s on average. The peak westward electric fields during stage-1 expansions range from 1.1 to 24 mV/m and are 7.4 mV/m on average. The corresponding peak earthward meridional flows range from 6 to 272 km/s and are 62.4 km/s on average. Peak westward electric fields during stage-2 expansions range from 2.5 to 19 mV/m and are 9.8 mV/m on average.

Table 4. Wave Poynting Vectors

		Onset Trigger Power, μW/m^2				Peak Power, μW/m^2				
Event	Orbit	Step	$\hat{V}$	$\hat{D}$	$\hat{B}_o$[a]	Step	$\hat{V}$	$\hat{D}$	$\hat{B}_o$[a]	P_i[b] mW/m^2
A	461	3	+1.5	−9	+2	5	+0	+135	+380	199
						6	+0	+0	+17	10
B	481	3	+1.2	+0	+1.2	5	+2	−2	+170	67
						6	−38	−20	+225	115
C_α	484	4	−1	+0	+40	4	−1	+0	+40	28
C_β		4	+0	+0	+9	5	−3	+39	+50	33
D	540[c]	3	+0	+0	+1	4	−2	+2	+62	16
E	540	3	+0	+0	+10	4	+50	+130	+780	183
F	545[c]	3	+0	+0	+3	3	+0	+0	+3	1
G	545	4	+0	−3	+47	4	+0	−3	+47	14
						6	+15	+30	+150	42
H	545	3	+40	+33	−15	4	−70	−133	+1300	362
						6	+8	+12	+112	27
I	546[d]	3	+0	+0	+2	5	−80	+0	+55	29
						6	−14	+2	+30	15
J	547	3	+0	−1	+15	5	+5	−5	+75	26
						6	+140	−390	+710	269
K	547	3	+0	+0	+0	5	+0	+60	+400	147
L	547	3	+0	+0	+2	4	+0	−87	+295	98
M_α	550	3	+1	+0	+1	5	−47	+150	+125	44
M_β		4	+0	+23	+85	4	+0	+23	+85	30
						6	+0	+0	+10	3
N	552	3	+0	+0	+2	4	−8	+75	+175	68
						wedge				
O	553	3	+5	+0	+10	5	+400	+150	+700	428
						6	−50	+35	+25	17
P_α	572[d]	4	−8	−25	+50	4	−8	−25	+50	29
P_β		4	−15	+12	+97	4	−15	+12	+97	50
						6	−5	−1	+63	30
Q	577	3	+0	+0	+3	5	+20	+15	+38	16
						6	+20	+0	+85	29
R_α	583	3	+1	+2	+23	5	−8	+3	+235	115
R_β	583	4	+19	+0	+80	4	+19	+0	+80	40
S_α	586[d]	3	−5	+10	+15	4	−4	+18	+35	12
S_β		4	+16	+6	+72	4	+16	+6	+72	23
						6	−18	+16	+55	18
T	593	3	+7	+0	+35	6	−50	−180	+300	124
a	547					EFB	+25	+85	+120	44
b	547					EFB	−3.5	+60	+200	72
c	572					EFB	−25	+10	+27	12

[a]Positive if toward the ionosphere, negative if away.

[b]Determined by multiplying the measured downward power by 55,000 nT/$|B|$.

[c]Pseudobreakup.

[d]At the western edge of onset sector.

Corresponding peak earthward flows range from 26 to 206 km/s and are 68 km/s on average. EFB electric fields range from 3 to 13.2 mV/m and are 8.5 mV/m on average. Corresponding earthward flows ranged from 18 to 138 km/s and are 79.9 km/s on average. Again, we remind the reader that these observations were made significantly away from the magnetic equator. Equatorial bulk flow speeds can be much higher, for example, electric and magnetic fields of 10 mV/m and 25 nT, respectively, yield an $\mathbf{E} \times \mathbf{B}$ drift speed of 400 km/s.

4.4. Wave-Power Vectors

As seen in Tables 4 and 5, approximately 90% of the wave power, on average, is contained in the component

Table 5. Wave Power Vector Statistics

Stage	Count	$\langle P_\parallel/P \rangle$	$\langle P_\parallel \rangle$[a]	$P_{\parallel,\max}$[a]	$\langle P_i \rangle$[b]	$P_{i,\max}$[b]
Onset trigger (step 3, 4)	24	0.90	25	97	11	50
Onset trigger (step 3)[c]	16	0.87	8	35	3	14
LEXO (step 4)	23	0.93	180	1300	63	362
LEXO/stage-1 peak (step 4, 5)	23	0.92	230	1300	89	428
Stage-2 peak/EFB[d] (step 6, EFB)	15	0.89	142	710	55	269

[a]Units are $\mu W/m^2$.
[b]Units are mW/m^2.
[c]Excluding LEXOs.
[d]EFB, earthward flow burst.

flowing toward the ionosphere along the background magnetic field. Figures 12–14 contain plots of the perpendicular components, $\delta \mathbf{S}_\perp$, of the waves for which the statistics are provided in Table 5 for the 20 events. Values are listed in Table 4 for the onset trigger power and for peak power for stage 1 (steps 4 and 5) and for stage 2 (step 6). The vectors are plotted on a common plane perpendicular to the magnetic field with the sunward direction at the top. Trigger (step 3) and LEXO (step 4) waves have $\partial E_D/\partial t$ eastward while power flows toward the ionosphere. The FACs carries by these waves have region-2 sense. Stage-1 (step 5), stage-2 (step 6), and EFB waves have $\partial E_D/\partial t$ westward while power flows toward the ionosphere. The FACs carries by these waves have region-1 sense. Assuming the waves are azimuthally plane polarized, we use the magnetic deflections to determine in which quadrant with respect to a wave's centroid that CRRES is located in the plane. The locations of the base of the vectors within a quadrant are also guided by the relative strengths of the deflections of the magnetic components.

Figure 12 plots $\delta \mathbf{S}_\perp$ of the onset trigger waves. This figure dramatizes the fact that CRRES does not detect wave power arriving from the outside prior to the start of dipolarization (local onset). Figure 13 plots $\delta \mathbf{S}_\perp$ of the LEXO waves. Note that although the placement is done completely independent of the perpendicular vector power direction, vectors tend to point away from the wave centroids, providing an average pattern for this substorm onset feature. The three exceptions (M_α, O, and R_β) probably occur because an adjacent wavelength of the drift-ballooning wave is dominating. In all cases the primary perpendicular power is azimuthal with no significant earthward component. Since $\mathbf{j} \cdot \mathbf{E} < 0$ for trigger and LEXO waves, and the wave power is predominantly field aligned, we assume a local source for that power. The pattern consistency with vectors em-

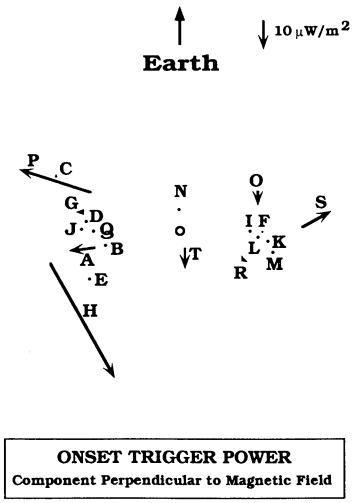

Figure 12. Perpendicular component of the wave-power vectors of the onset trigger waves listed in Table 4 placed with respect to each wave's centroid.

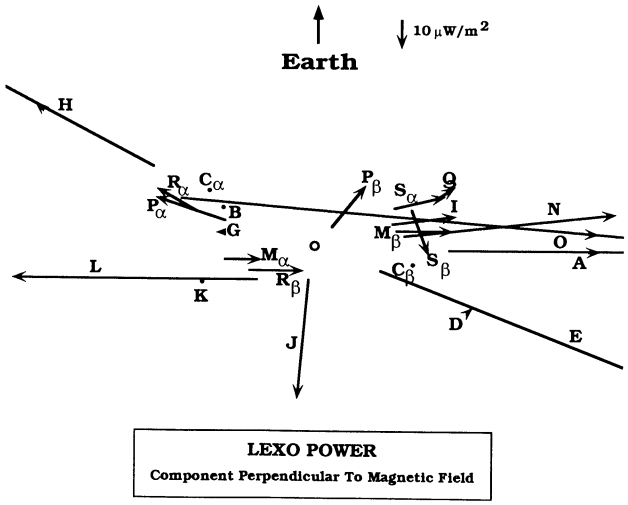

Figure 13. Perpendicular components of the wave-power vectors of LEXO waves at maximum eastward electric field placed with respect to each wave's centroid.

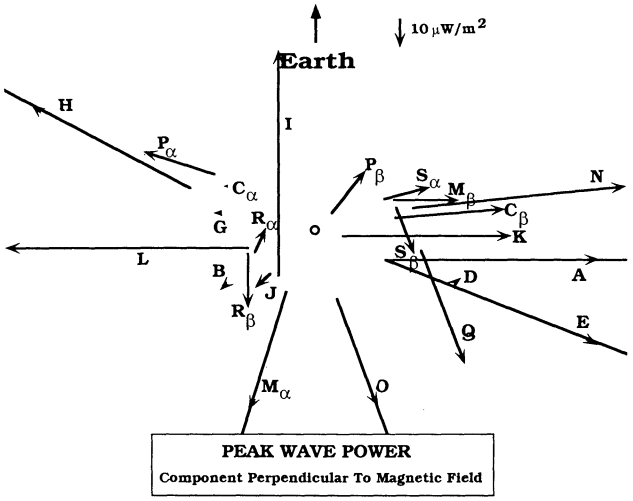

Figure 14. Perpendicular component of the wave-power vectors at peak parallel power for the LEXO/expansion waves listed in Table 4 placed with respect to each wave's centroid.

anating from the centroids confirms a local source for wave power release.

Figure 14 gives a similar plot for the LEXO/stage-1 expansion wave at peak power. Again, the placements and the resulting pattern of power away from the centroid organize into a picture of a local source whose internal consistency confirms the directions calculated for the wave-power vectors. The pattern is more symmetric about the wave centroids than seen for the LEXO waves alone. There are several vectors that predominantly point tailward away from the centroids.

Figure 15 is a similar plot at peak power for stage-2 expansions (including event T and EFBs). Notice the lack of organization around the centroid compared with Figures 13 and 14. There is a sense of average inward direction to the vectors. The magnitudes of the vectors are also smaller. This is consistent with our contention that stage-2 expansions are different in character from onset and LEXO. Specifically, while mode conversion (like flow braking) is taking place nearby, the source of the wave power is nonlocal since locally $\mathbf{j} \cdot \mathbf{E} > 0$ during stage-2 expansions and EFBs.

4.5. Observations Outside the Onset Sector

In addition to the events witnessed by CRRES within the onset sector, a similar, but larger number of events occurred just to the west of the onset sector. When CRRES is west but near the onset sector, an energy release is observed as the upward leg of the SCW arrives at the satellite. That is, before the westward expansion electric field enhances at CRRES, the electric field turns eastward and a burst of power is observed flowing toward the ionosphere similar to a LEXO wave (step 4). Presumably, this represents a local contribution to the power in the early stage of a WTS.

Events observed to the east of the onset sector, in the region of the downward leg of the SCW, lack the sharpness of detail seen within and west of the onset sector, and less power is observed flowing toward the ionosphere. Observations within the downward side of the SCW, such as those following the end of event P and also in the event (orbit 491) discussed by *Maynard et al.* [1998a], are typical. This is not surprising, for two reasons. First, downward FACs are carried by upflowing electrons. These are readily available from the ionosphere. The large field-aligned potential drops to accelerate auroral electrons, typical of the upward current regions, are not required. Second, we see that the waves responsible for the energy release toward the ionosphere propagate to the west. Under most IMF conditions, there is not a feature on the eastward side of the SCW comparable to the surge seen on the westward side of the SCW sector.

5. Discussion

CRRES observations of substorm onsets, within the local-time sector across which the SCW first appears, support the NGO model and contradict the NENL model in 19 of the 20 events. Specifically, the observations are consistent with drift-Alfvén ballooning as the mechanism of substorm onset. Within the NGO model scenario presented here, much substorm phenomenology finds a degree of clarification. We describe this model based on the observations presented above and then compare the results with other observations.

5.1. An Observationally Based NGO Model of Substorms

Figure 16 shows meridional cross sections of the magnetosphere depicting substorm onsets and expansions, based on CRRES and correlated ground observations. Figure 2 schematized the typical observations associ-

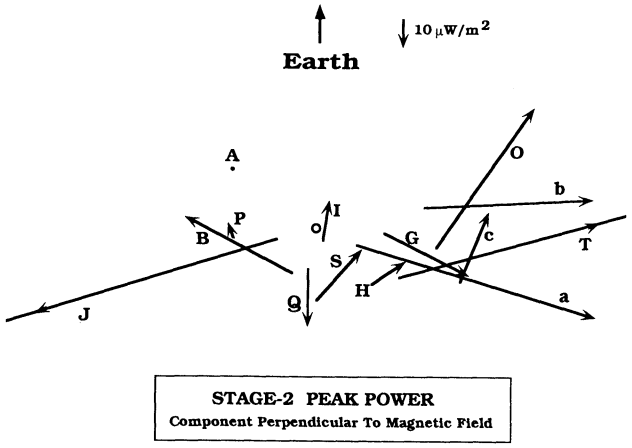

Figure 15. Perpendicular component of the wave-power vectors at peak parallel power during stage-2 expansions and EFBs listed in Table 4 placed with respect to each wave's centroid.

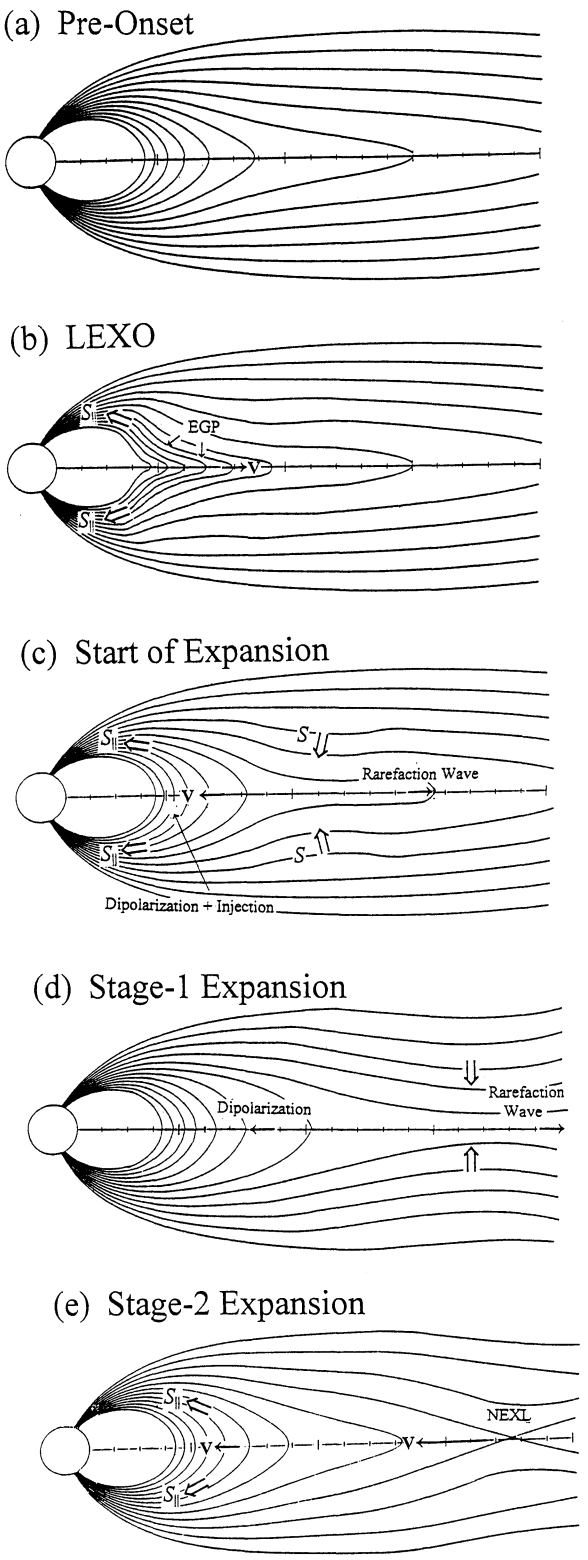

Figure 16. Meridional depiction of how substorms evolve in NGO morphology according to CRRES observations from the (a) preonset configuration through (b) LEXO, and (c) the start of stage-1 expansion. (d) A rarefection wave is launched downtail, which stimulates one or more NEXLs downtail, resulting in (e) a stage-2 expansion as fast bulk flows emanating from a NEXL arrive in the inner magnetosphere.

ated with onset and expansion. This provides the framework event sequence for Figure 16.

During the growth phase a background dawn-dusk electric field develops and quasi-electrostatic oscillations in the Pi2 frequency band occur. We suggest that these oscillations are drift waves that tap the free energy available from the earthward pressure gradient of ring-current ions. Trigger waves occur as the amplitudes of the drift waves grow, causing reversals of the total electric field to dusk-dawn. At these times, $\mathbf{j} \cdot \mathbf{E} < 0$, and the drift wave couples to the Alfvén mode, converting plasma kinetic energy into electromagnetic energy that flows toward the ionosphere. We refer to this phenomenon as drift-Alfvén ballooning (DAB). This may occur in the absence of an external trigger; however, external triggering may couple with DAB, as we discuss later.

Upon reflection of trigger waves from the ionosphere, the magnetic configuration is nearly restored. However, some energy is dissipated as Joule heat in the ionosphere and some is still contained in the waves. When the energy is removed from the plasma by this process faster than plasma is energized by the background (growth-phase) electric field, cross-tail current is reduced, the magnetic field starts to dipolarize, and the SCW first appears. On the ground, there is a Pi2 onset, a westward electrojet intensifies, and a magnetic bay begins. If this is not followed by LEXO, then a pseudobreakup results. However, in most of the onsets we observed LEXO does follow, and the trigger wave has caused onset of at least a small substorm. The power released by trigger waves increases explosively at LEXO (Figure 16b). Figure 16b, based on CRRES observations, is basically the same as depicted by *Hurricane et al.* [1999] as the meridional magnetic structure at "substorm detonation." During LEXO, energy is released from drifting plasma at a rate far exceeding the rate of growth-phase energization. The outward displacement of flux tubes is a significant fraction of the local equilibrium scale length. For example, an eastward electric field of 10 mV/m lasting for 30 s in a 50-nT magnetic field produces a displacement of $\sim 1\ R_E$. The configuration does not relax to near its previous state as the electric field turns westward. Rather, it significantly overshoots the prior equilibrium, leaving a pressure reduction in its wake, and a rarefaction wave is launched tailward (Figure 16c). During LEXO and the start of this stage-1 expansion, appreciable magnetic compression is observed. This suggests that the equilibrium is disrupted, resulting in a fast-mode collapse of the configuration and launch of the rarefaction wave. Power flowing toward the ionosphere often continues to increase as the electric field turns westward. The source of the power flowing toward the ionosphere has switched from the $\mathbf{j} \cdot \mathbf{E} < 0$ local conversion of plasma kinetic energy to a nonlocal source, probably stress reduction of the magnetic field as the rarefaction wave passes downtail, leaving a more dipolar configuration in its wake (Figure 16d).

DAB waves continue into the expansion phase. *Roux et al.* [1991] correlated similar structures in the geosynchronous plasma sheet to WTSs. While power flows toward the ionosphere on average, parallel power can be observed locally as flowing in either direction. Whenever the electric field turns eastward as a ballooning wave passes by, while net power is reflected power flowing away from the ionosphere, the substorm electrojet wanes or turns off completely. Even in the absence of such interference, there is a limited amount energy available from the near-Earth magnetosphere to power substorm expansion without invoking magnetic reconnection. However, the available energy is enough to account for small substorms. Usually, however, a stage-2 expansion is subsequently observed.

While apogee of CRRES is too low to witness how expansion proceeds poleward in the auroral zone, the different signatures of stage-1 and stage-2 expansions permit us to speculate on the nature of that process. We assume that tailward propagating rarefaction waves activate NEXLs in the near-Earth to midtail plasma sheet as depicted in Figure 16e. Poleward expansion can continue into the polar cap as the NEXL reconnects lobe flux. Expansion can stop short of the polar cap if the NEXL deactivates before reaching the lobe (as in event A). In the inner magnetosphere a stage-2 expansion appears as an enhancement of westward electric field and dipolarization but without the LEXO wave. A stage-2 expansion may be nearly contiguous to stage-1, and thus it might not be discerned as a separate event. For example, the expansion of event E (see M96) was sustained long enough and the ground magnetic bay was large enough that a NEXL most likely activated. However, while the expansion started with a LEXO, two separate expansions are not obvious in either CRRES or ground data.

5.2. NGO Versus NENL Models of Substorm Onset

Simulations of NENL-induced onsets [*Birn and Hesse*, 1991; *Birn et al.*, 1999] suggest that earthward flow emanating from a NEXL causes magnetic flux to pile up in the inner magnetosphere. The SCW exists consistent with this dipolarization, arising from the azimuthal pressure gradient and/or the vorticity present along the edges of the flow channel. As discussed by *Shiokawa et al.* [1997], the braking of earthward flow, which can be bursty, implies an eastward inertial current that results in both the reduction of cross-tail current and the conversion of flow kinetic energy into electromagnetic energy flowing toward the ionosphere by Alfvén waves carrying FAC of region-1 (SCW) sense. In the braking scenario the electric field does not turn eastward, but remains westward while the convective derivative dE_D/dt is eastward. The initial current diversion related to the eastward inertial current associated with the braking lasts a few minutes and only contributes a portion of the total substorm current diversion near Earth. Modifications of pressure gradients provide the more dominant and sustained contributions to the SCW [*Shiokawa et al.*, 1998; *Birn et al.*, 1999].

CRRES observations, taken within the local-time sector across which the SCW initially appears, are consistent with the description illustrated in Figures 2 and 16 and discussed above. Referring to Figure 1, that description has NGO morphology. With the possible exception of event T, the observations not only are consistent with NGO morphology, but also directly contradict the causal link between the NEXL and the SCW within the NENL onset model in three related ways. First, CRRES observations invariably show that the first signs of activity preceding onset are associated with eastward excursions of the electric field. The initial significant low-frequency wave power observed flows toward the ionosphere and is associated with eastward electric field. The explosive increase in power delivered to the ionosphere at LEXO occurs as the electric field becomes eastward. Enhanced background westward electric field appears following LEXO. The trigger waves and LEXO are the first contradiction with the NENL onset model. Second, dipolarization is observed to begin and the SCW first appears as a consequence of the energy release associated with eastward excursions of the electric field. The third contradiction is even more blatant. The explosive increase of the power flowing toward the ionosphere is observed to begin at LEXO while E_D is eastward and plasma begins to accelerate tailward. In about half of the events, power maximizes at peak eastward electric field during LEXO. In the remaining events the power continues to increase as the electric field turns westward at the start of stage-1 expansion and maximizes before or at peak westward electric field. In these cases, power toward the ionosphere is increasing while plasma is accelerating earthward, not while the plasma is braking. During stage-2 expansions and EFBs, even while $\partial E_D/\partial t$ is westward when the power flowing toward the ionosphere is observed to increase, the convective derivative dE_D/dt may be eastward, consistent with driving from the tail. This cannot be so at LEXO and the start of stage-1 expansion.

Generally, we recognize that there may be different paths by which the global instability known as the magnetospheric substorm begins. This may have NGO or NENL morphology. NEXL formation has been observed in close temporal proximity to ground onset and even a few minutes before [e.g., *Sergeev et al.*, 1995; *Ohtani et al.*, 1999]. Our observations are 95% in favor of NGO morphology, but we must note that during storm times, high background activity both over auroral stations and at CRRES prevented substorm onset identification except in a few cases.

Baumjohann et al. [1996] suggested a distinction between storm-time and non-storm-time substorms. They performed a superposed-epoch analysis of 40 substorms observed at radial distances between 10 and 19 R_E by the AMPTE/CCE satellite, separating storm-time sub-

storms from non-storm substorms. They found that storm-time substorms behaved more consistently with expectations from the NENL model than did nonstorm substorms and suggested that nonstorm substorms were consistent with NGO morphology. The single CRRES event (event T) that might satisfy NENL onset morphology occurred during the March 1991 storm.

Consider the typical substorm expansion onset observed at CRRES and summarized in Figure 2. We note that from an observing platform in the near magnetotail, say, $X < -20\ R_E$, steps 1–4 illustrated in Figure 2 would not be seen. The observations will be dominated by signatures of NEXL formation: for example, bipolar magnetic field signatures and fast bulk flows. These observations would precede or coincide with a major bay intensification and poleward expansion. Such major intensifications during multiple-onset events have been referred to by some as "main substorm onsets" [e.g., *Hsu and McPherron*, 1998] and are associated with lobe reconnection. From this vantage, the earlier Pi2 onset and magnetic bay illustrated in Figure 2 and seen in event P could be mistakenly interpreted as a pseudobreakup when it was actually onset. What could have occurred was a stage-1 expansion onset, triggering NEXL formation and resulting in fast, earthward bulk flows, which we recognize as a stage-2 expansion.

5.3. M-I Coupling, Pseudobreakups, and Substorms

Several observational studies suggest that the physical processes leading up to pseudobreakups and substorm onsets are similar [e.g., *Elphinstone et al.*, 1995; *Koskinen et al.*, 1993; *Pulkkinen*, 1996; *Rostoker*, 1998] and are only distinguished by subsequent poleward expansion in the latter case. *Nakamura et al.* [1994] suggest that they may also be distinguished by the size of the magnetospheric source. M96 suggested that M-I coupling plays a critical role in determining whether eastward excursions of the electric field (trigger waves) result in a substorm onset or merely a pseudobreakup. They also noted the interference phenomenon (step 7) reported here. In one event, when wave power released toward the ionosphere during a dusk-dawn electric field excursion did not return to CRRES, a local dipolarization failed to expand and a pseudobreakup occurred. In a second event a portion of the wave power released toward the ionosphere returned to CRRES in phase with the magnetospheric electric field oscillations, and a substorm expansion followed. In the third event a substorm expansion was in progress when wave power returned to CRRES from the ionosphere but was out of phase with the magnetospheric electric field oscillations, as in step 7 of Figure 2. The substorm electrojet turned off momentarily until the parallel wave power and (Pi2 band) electric field oscillations returned to phase.

The electric fields of drift waves we observe have periods ranging from about 60 to 90 s. Table 2 shows that for the 17 substorm onsets (excluding the two pseudobreakups and event T) the separation between local onset and LEXO is greater than one period in eight events and one period or less in nine events. Two events are dual onsets in which LEXOs occur at consecutive periods. In the latter category, three events are dual onsets in which LEXOs do not occur at consecutive periods and exhibit interference in between. Therefore, in 11 of the 17 events, onset triggers and LEXOs occur at consecutive periods of the DAB wave, and the average separation for the 17 events is 1.6 ± 1.0 min. The interference phenomenon also requires the presence of a trigger-like wave and power reflected from the ionosphere. Thus the larger database used in this study supports the contention made by M96 that M-I coupling plays a critical role in differentiating substorm onsets from pseudobreakups.

Elphinstone et al. [1995] used Viking images to describe azimuthally spaced auroral forms (AAFs) usually present prior to the explosive poleward motion associated with optical substorm onset. AAFs are frequently observed along the equatorward band of the UV aurora with azimuthal mode numbers ranging from 30 to 135. AAFs can occur before strong Pi2 activity and before geosynchronous-orbit particle injection. Precursor activity associated with AAFs was also seen near geosynchronous orbit. Some of these precursors might be considered pseudobreakups. AAFs brighten in conjunction with substorm onset, which led Elphinstone et al. to suggest that they represent growth-phase activity causally related to substorm onset, specifically Alfvén ballooning. They report that the region of brightening at onset is typically 1-hour wide. We suggest that these AAFs are the optical manifestations of trigger/LEXO waves. Ion average energies at CRRES are typically around 40 keV. *Roux et al.* [1991] estimated an ion gradient drift velocity of about 100 km/s corresponding to this energy. This speed compared favorably with the speed of WTSs observed conjugate to their geosynchronous orbit observations. Azimuthal phase speed of 100 km/s and the 60- to 90-s period oscillations of the dawn-dusk component of the electric field observed at CRRES during the growth phase correspond to azimuthal mode numbers ranging from 30 to 44. Slower phase speeds yield higher mode numbers. Consider coupling of adjacent wave periods. For an Alfvén wave travel time to the ionosphere and back of 2 min and a phase speed of 100 km/s, the width of the onset sector would be roughly 1.9 R_E wide at geosynchronous orbit, or about 1-hour wide. While these estimates compare favorably with the findings of Elphinstone et al., they should not be regarded as definitive. While we can estimate the ion gradient drift speed, without multiple satellites we do not know the phase speed of the observed DAB waves.

5.4. Pi2s, the SCW, and FAC Filaments

It is generally believed that auroral Pi2s associated with substorm onset represent the leading edge of the substorm FAC and subsequent reflections. (See the re-

view by *Olson* [1999, and references therein].) CRRES data suggest that the 60- to 90-s oscillations of the electric field observed at near-geosynchronous altitude are directly related to auroral Pi2s. When these oscillations reverse the total electric field to dusk-dawn, electromagnetic energy flows toward the ionosphere. Weak trigger waves may be responsible for low-level Pi2 activity preceding auroral onset. Stronger trigger waves and LEXOs are responsible for auroral Pi2 onsets at substorm onsets or pseudobreakups. M96 noted specific correspondences between weak Pi2 wave trains observed over the Russian sector and trigger waves during orbits 535 (during which a pseudobreakup occurred) and 540 (surrounding events D and E). In the present paper we noted a close correlation between LEXOs observed at CRRES and Pi2 onsets over Oulu during event P.

The SCW appears in our data following one or more trigger waves and before the appearance of enhanced westward electric fields and earthward flows. We contend that reduction of the cross-tail current at local onset, and hence growth of the SCW, results as plasma kinetic energy is converted into electromagnetic energy carried by trigger waves during eastward excursions of the electric field. This spans several wavelengths across azimuth as compared with the transient FAC filaments carried by individual trigger and LEXO waves. Following local onset, the SCW is maintained by enhanced earthward flows as described within global MHD simulations or the modeling of, for example, *Birn et al.* [1999]. The transient behavior resulting from ballooning waves continues into expansion. As we have noted earlier, such ballooning behavior also appears as the SCW expands over CRRES and would correspond to the head of a WTS early in its expansion [*Roux et al.*, 1991]. *Hoffman et al.* [1994] found that while net upward FAC sufficient for electrojet closure is contained in the surge, the FACs are very filamentary. Either sign of auroral FAC can be encountered locally. We suggest that the ballooning behavior we observe contributes to the transient behavior of FACs within the substorm surge. Fluctuations in reconnection rates at NEXLs and consequent earthward plasma flows may also contribute to FAC variability within the surge.

5.5. Low-Frequency Behavior Associated With Onsets and Expansions

Roux et al. [1991] invoked drift-Alfvén ballooning to explain the observation of electric field oscillations and successive FAC filaments of alternating direction passing over the GEOS 2 spacecraft during a substorm expansion. Using conjugate ground observations, they related these ballooning waves to WTSs. *Holter et al.* [1995] performed spectral and wavelet analyses to characterize the transient oscillations observed during the Roux et al. event. They found long 300-s-period oscillations, observed after breakup, which they interpreted as second harmonic modes corresponding to oscillations of the whole field line. They also note two shorter periods of 45 and 65 s, which they interpret as waves trapped in the current layer localized close to the magnetic equator. These were observed during breakup only. The 45-s-period oscillation involved mainly the magnetic field; E_D had vanishing small amplitude at this frequency. The 65-s oscillations occurred after the field had partially dipolarized. E_D had relatively large amplitude at this frequency. Evidence of a fast magnetosonic mode occurred at dipolarization/injection. *Cheng and Lui* [1998] examined an event consisting of an EGP, onset, and current disruption observed with AMPTE/CCE. They found a low-frequency instability with period about 50–75 s excited 2 min before current disruption. Their theoretical analysis of a kinetic ballooning instability yielded a resonance between the wave and the ion magnetic drift which accounts for the ~30-s enhancement of duskward ion flux observed during the EGP, which may then excite higher frequencies such as the cross-field current instability [*Lui et al.*, 1990].

At CRRES, three low-frequency oscillations are routinely observed. Beginning tens of minutes before onset, E_D oscillates in the Pi2 band at periods between 60 and 90 s. The trigger waves, and eventually onset, grow from these oscillations. The shorter-period oscillations in the magnetic field occur primarily with a period of 30 s. (These are not apparent in the 15-s averaged data presented here but are obvious in 5-s data, usually present in all components of $\mathbf{B}$ as well as $|\mathbf{B}|$.) This oscillation turns on in association with the start of dipolarization following a trigger wave and persists into the first stage of expansion. As discussed in the next section, the EGP magnetic signature seen at CRRES is clearly related to this oscillation. Long-period (up to 300 s) oscillations of the magnetic field (mainly in the D component) are often observed during stage-1 expansions. We interpret these oscillations as resulting from passage of WTSs over the satellite. However, at this time the period of the E_D oscillation is closer to 2 min. During stage-1 expansions, while the main wave power flows toward the ionosphere on average, that power usually oscillates at periods from about 150 to 200 s. Event A (Figure 6) and event E (M96, Figure 14) provide examples. Event N was atypical in that the preonset E_D oscillations occurred at a shorter period than usual, ~45 s. Magnetic oscillations occurred with a 50-s period. Both were apparent for tens of minutes prior to onset. This event exhibited 13 trigger waves prior to LEXO, occurring every 45 to 90 s. Other events had four or fewer trigger waves. LEXO precedes westward electric field enhancement, rapid dipolarization, and injection. During this interval a major magnetic compression occurs in conjunction with EGP signatures, suggestive of a fast-mode collapse of the near-Earth, quasi-equilibrium configuration.

5.6. The Explosive Growth Phase

Ohtani et al. [1992] noted two categories of signatures surrounding local onsets observed by AMPTE/CCE,

distinguished by whether current disruption presumably occurred earthward (type I) or tailward (type II) of the satellite. The EGP occurred during type-II events and was interpreted as resulting from an explosive increase of the cross-tail current tailward of the AMPTE/CCE satellite. They noted that they did not see the expected signatures of an "anti-EGP" in the type-I events. We suggest a different interpretation of the EGP. A more complete discussion of the EGP will be provided in a separate report. Here we summarize. First, the EGP is an onset phenomenon, not a precursor to local onset. Second, the EGP does not represent an increase of cross-tail current tailward of the satellite but is the magnetic perturbation owing to the LEXO/ballooning wave. In CRRES 5-s magnetic field data, it is clear that the EGP is a "hiccup" during a half cycle of the 30-s **B** oscillation which turns on in association with dipolarization, as noted earlier. In the 15-s data presented here, the EGP occurs in association with LEXO and eastward electric field. Large amplitude of the complementary half cycle of the 30-s oscillation, i.e., an "anti-EGP" in which the H component increases and $|V|$ increases, can also be seen in the data on occasion. Magnetic compression accompanies this oscillation, and hence the EGP appears to be a symptom of the ballooning phenomenon (see also *Bhattacharjee et al.* [1998] and *Ma and Bhattacharjee* [1998]). From analysis of a kinetic ballooning instability, *Cheng and Lui* [1998] suggest the increase in duskward flux of energetic ions observed with AMPTE/CCE at the time of the EGP results from a resonance between ions and the ballooning wave. They are the carriers of the eastward polarization current associated with the wave while $\partial E_D/\partial t$ is eastward (C. Z. Cheng, private communication, 2000), which we have termed the LEXO wave.

5.7. Bursty Bulk Flows

Angelopoulos et al. [1992] define bursty bulk flows (BBFs) as segments of continuous ion flow magnitude above 100 km/s in the central plasma sheet, during which the bulk flow exceeds 400 km/s for at least one sample period. For the purposes of this discussion we consider only earthward fast flows. The CRRES observations presented here were made significantly off the magnetic equator, where the magnetic field averaged about 150 nT. Peak expansion electric fields around 10 mV/m are observed. If viewed near the magnetic equator, and perhaps a bit farther out, where the magnetic field magnitude is 25 nT or lower, say, 8 or 9 R_E, stage-1 expansion flows would qualify as containing BBFs. Stage-2 expansion flows are probably fast flows spawned in the near-Earth tail by reconnection. The other fast earthward flows observed are the EFBs. They are rare at CRRES's location, have 1-min duration, and occur during local recovery. From the short list of about 50 events and 100 hours of data, from which the events in Table 1 were determined, we found three isolated EFBs. They appear to be the near-geosynchronous remnants of BBFs which were spawned during a short burst of reconnection during recovery.

Using observations from the AMPTE/Ion Release Module (IRM) satellite, *Shiokawa et al.* [1997] find that the occurrence frequency of earthward high-speed ($\geq$400 km/s) ion bulk flows minimize at $X \approx -12\ R_E$. The observed decrease in occurrence as X increases from apogee ($X \approx -19\ R_E$) to $-12\ R_E$ could be fit to a model calculation of flow braking. The model calculations, of course, indicate that the occurrence rate should continue to decrease rapidly for $X > -12\ R_E$. The relatively rare occurrence of EFBs in the CRRES data would be consistent with this model. However, the AMPTE/IRM observations show that the occurrence frequency increases significantly from $X \approx -12$ to perigee at $X \approx -9\ R_E$. We suggest that the increase in the occurrence frequency for $X > -12\ R_E$ results from LEXOs and stage-1 expansion starts in the near-geosynchronous plasma sheet.

5.8. Triggering of Substorms

Repeated investigations support the notion that a large percentage of substorm onsets are triggered by reduction of the solar wind driver [e.g., *Rostoker*, 1983; *McPherron et al.*, 1986]. *Lyons* [1995] suggests that all substorms are triggered in this manner. For a few events listed in Table 1, solar wind data were available. We found no case which suggests that onset was triggered by a solar wind change. It should be noted that substorm onsets can occur in the absence of any trigger in the solar wind [e.g., *Henderson et al.*, 1996].

On the basis of global stress balance between the solar wind and magnetosphere, *Siscoe and Cummings* [1969] provided an explanation of why reductions of solar-wind-imposed stress should result in magnetospheric substorms. However, despite repeated investigations showing that substorms can be triggered by reductions of the solar wind driver, apart from Lyons's substorm model, no satisfactory direct causal link has been given to account for such triggering within either the NGO or NENL substorm onset hypotheses. Such a causal link would serve as strong testimony in favor of an onset hypothesis.

The drift-wave nature of the onset scenario suggested by the CRRES observations provides a natural framework within which to account for substorm triggering. The cross-tail electric field is the superposition of the drift waves (δE_D) and the background westward electric field (E_o) owing to the solar wind driver. Specifically, $E_D = E_o + \delta E_D\,(t)\, e^{i(k_y y - \omega t)}$. We have found that substorm activity is initiated by the release of energy from the plasma sheet when the electric field turns eastward. This can occur without an external trigger as the amplitude of $\delta E_D(t)$ grows so as to exceed the value of E_o. Alternatively, a reduction of E_o, corresponding to an external trigger, can result in eastward excursions of the electric field when the drift waves are present. Related to this process, *Hurricane et al.* [1999] suggest

"substorm detonation" can occur when an external trigger causes a sufficient (ballooning) displacement of flux tubes. Finally, it is conceivable that during strong solar wind driving, while the amplitudes of drift waves might grow from time to time sufficient to reverse the total electric field, kinetic energy cannot be removed from plasma in the inner plasma sheet at a rate fast enough compared with the rate at which the background convection energizes the plasma to permit disruption of the quasi-equilibrium. The result could be a convection bay or "steady magnetospheric convection" event [*Sergeev et al.*, 1994; *Yahnin et al.*, 1994].

6. Summary

We have analyzed 20 events in which the CRRES satellite was positioned in the near-geosynchronous plasma sheet within the local-time sector defined by the SCW at onset. In spite of phenomenological complexity we found seven characteristic features of substorm onsets and expansions observed by CRRES. These are illustrated in Figure 2. Generally, the SCW forms in the absence of an enhancement of earthward bulk plasma flow or wave power flowing into the region from the outside. Indeed, observations of local onset in 19 of the 20 events directly contradict the notion that the SCW is initiated by the braking of enhanced earthward bulk flow as contained in the near-Earth neutral line model. Rather, these observations are consistent with the near-geosynchronous onset model and drift-Alfvén ballooning. Ballooning arises as quasi-electrostatic drift waves, which can be present for tens of minutes prior to onset, couple to the Alfvén mode during eastward excursions of the electric field ($\mathbf{j} \cdot \mathbf{E} < 0$). Dipolarization usually begins gradually following such trigger waves. M-I coupling plays a role to differentiate pseudobreakups from expansion onsets. In the latter case, within a few minutes from when dipolarization begins (local onset), LEXO occurs. An EGP occurs in concert with tailward plasma flow and surge-sized power flowing toward the ionosphere at LEXO. The EGP is a "hiccup" during a half cycle of a 30-s $\mathbf{B}$ oscillation which turns on in association with dipolarization. Large amplitude of the complementary half-cycle of the 30-s oscillation, i.e., an "anti-EGP" in which the H component increases and $|V|$ increases, can also be seen in the data on occasion. Magnetic compression accompanies this oscillation, and hence the EGP appears to be a symptom of the ballooning phenomenon.

Expansions often occur in two stages. The first stage follows LEXO and appears consistent with fast-mode collapse of the near-Earth configuration. Particle injection occurs at this time. The second and later stages of expansion result from earthward flow enhancements, as might be expected from activation of a NEXL. When west but near the onset sector, as the upward leg of the SCW arrives, but before expansion enhancement of westward electric field, the electric field turns eastward, and a burst of power flowing toward the ionosphere and an EGP signature similar to LEXO are observed. Presumably, this power is contributing to the early stage of a WTS. Events observed east of the onset sector, in the region of the downward leg of the SCW, lack sharpness of detail and involve less wave power compared with observations within or west of the onset sector.

Near-geosynchronous substorm onsets provide an explanation for the increase in the occurrence rate of BBFs earthward of $X \approx -12\ R_E$ seen in the data of *Shiokawa et al.* [1997]. Drift-Alfvén ballooning also provides a possible causal link between reductions of the solar wind driver and substorm onsets.

Acknowledgments. This project was supported by NASA under contract NASW-96-007 and grant NAG5-9110 and the U.S. Air Force Office of Scientific Research under task 2411PL04 and grant F49620-98-1-0012. The authors are grateful for helpful discussions with J. Hughes, A. T. Y. Lui, P. Rothwell, G. Siscoe, and R. Wolf. J. Samson provided useful comments, encouragement, and CANOPUS data. A. Yahnin provided Russian magnetometer data, provided a preliminary catalog of *AE*, and was an integral part of the background studies leading to this paper. We thank the institutes who maintain the IMAGE magnetometer array for use of their data. We thank I. R. Mann and D. K. Milling for SAMNET data. Some magnetometer data came from STEP Project 6.4, provided by the National Geophysical Data Center. The CANOPUS array is supported by the Canadian Space Agency. The CRRES satellite was a joint U.S. Air Force and NASA mission. The electric field instrument was developed with the help of F. S. Mozer.

Janet G. Luhmann thanks the referees for their assistance in evaluating this paper.

References

Angelopoulos, V., W. Baumjohann, Kennel, F. V. Coroniti, M. G. Kivelson, R. Pellat, R. J. Walker, H. Lühr, and G. Paschmann, Bursty bulk flows in the inner central plasma sheet, *J. Geophys. Res., 97*, 4027, 1992.

Baumjohann, W., Y. Kamide, and R. Nakamura, Substorms, storms, and the near-Earth tail, *J. Geomagn. Geoelectr., 48*, 177, 1996.

Bhattacharjee, A., Z. W. Ma, and X. Wang, Ballooning instability of a thin current sheet in the high-Lundquist-number magnetotail, *Geophys. Res. Lett., 25*, 861, 1998.

Birn, J., and M. Hesse, The substorm current wedge and field-aligned currents in magnetohydrodynamic simulations of magnetic reconnection, *J. Geophys. Res., 96*, 1611, 1991.

Birn, J., M. Hesse, G. Haerendel, W. Baumjohann, and K. Shiokawa, Flow braking and the substorm current wedge, *J. Geophys. Res., 104*, 19,895, 1999.

Chao, J. K., J. R. Kan, A. T. Y. Lui, and S.-I. Akasofu, A model for thinning of the plasma sheet, *Planet. Space Sci., 25*, 703, 1977.

Cheng, C. Z., and A. T. Y. Lui, Kinetic ballooning instability for substorm onset and current disruption observed by AMPTE/CCE, *Geophys. Res. Lett., 25*, 4091, 1998.

Elphinstone, R. D., et al., Observations in the vicinity of substorm onset: Implications for the substorm process, *J. Geophys. Res., 100*, 7937, 1995.

Erickson, G. M., Substorm theories: United they stand, divided they fall, *U.S. Natl. Rep. Int. Union Geod. Geophys. 1991–1994, Rev. Geophys., 33*, 685–692, 1995.

Erickson, G. M., and R. A. Wolf, Is steady convection possible in Earth's magnetotail, *Geophys. Res. Lett., 7*, 897, 1980.

Erickson, G. M., R. W. Spiro, and R. A. Wolf, The physics of the Harnag discontinuity, *J. Geophys. Res., 96*, 1633, 1991.

Fairfield, D. H., and N. F. Ness, Configuration of the geomagnetic tail during substorms, *J. Geophys. Res., 75*, 7032, 1970.

Haerendel, G., Disruption, ballooning or auroral avalanche–On the cause of substorms, in *Substorms 1, Eur. Space Agency Spec. Publ., ESA SP-335*, 417, 1992.

Hardy, D. A., D. W. Walton, A. D. Johnstone, M. P. Gough, A. Huber, J. Pantazis, and R. Burkhardt, The low energy plasma analyzer, *IEEE Trans. Nucl. Sci., 40*, 246, 1993.

Hau, L.-N., R. A. Wolf, G.-H. Voigt, and C. C. Wu, Steady state magnetic field configurations for Earth's magnetotail, *J. Geophys. Res., 94*, 1303, 1989.

Henderson, M. G., G. D. Reeves, R. D. Belian, and J. S. Murphree, Observations of magnetospheric substorms occurring with no apparent solar wind/IMF trigger, *J. Geophys. Res., 101*, 10,773, 1996.

Heppner, J. P., A study of relationships between the aurora borealis and the geomagnetic disturbances caused by electric currents in the ionosphere, *Rep. DR135*, Def. Res. Board of Canada, Ottawa, Ontario, 1958.

Hoffman, R. A., R. Fujii, and M. Sugiura, Characteristics of the field-aligned current system in the nighttime sector during auroral substorms, *J. Geophys. Res., 99*, 21,303, 1994.

Holter, Ø., C. Altman, A. Roux, S. Perraut, A. Pedersen, H. Pécseli. B. Lybekk, J. Trulsen, A. Korth, and G. Kremser, Characterization of low-frequency oscillations at substorm breakup, *J. Geophys. Res., 100*, 19,109, 1995.

Hones, E. W., Jr., Transient phenomena in the magnetotail and their relation to substorms, *Space Sci. Rev., 23*, 393, 1979.

Hsu, T.-S., and R. L. McPherron, The main onset of a magnetic substorm, in *Substorms 4*, edited by S. Kokubun and Y. Kamide, pp. 79–82, Kluwer Acad., Norwell, Mass., 1998.

Hurricane, O. A., B. H. Fong, S. C. Cowley, F. V. Coroniti, C. F. Kennel, and R. Pellat, Substorm detonation, *J. Geophys. Res., 104*, 10,221, 1999.

Kan, J. R., A global magnetosphere-ionosphere coupling model of substorms, *J. Geophys. Res., 98*, 17,263, 1993.

Koskinen, H. E. J., R. E. Lopez, R. J. Pellinen, T. I. Pulkkinen, D. N. Baker, and T. Bösinger, Pseudobreakup and substorm growth phase in the ionosphere and magnetosphere, *J. Geophys. Res., 98*, 5801, 1993.

Lui, A. T. Y., Estimates of current changes in the geomagnetotail associated with substorms, *Geophys. Res. Lett., 5*, 853, 1978.

Lui, A. T. Y., A synthesis of magnetospheric substorm models, *J. Geophys. Res., 96*, 1849, 1991.

Lui, A. T. Y., A. Mankofsky, C.-L. Chang, K. Papadopoulos, and C. S. Wu, A current disruption mechanism in the neutral sheet: A possible trigger for substorm expansions, *Geophys. Res. Lett., 17*, 745, 1990.

Lyons, L. R., A new theory for magnetospheric substorms, *J. Geophys. Res., 100*, 19,069, 1995.

Lyons, L. R., T. Nagai, G. T. Blanchard, J. C. Samson, T. Yamamoto, T. Mukai, A. Nishida, and S. Kokubun, Association between Geotail plasma flows and auroral poleward boundary intensifications observed by CANOPUS photometers, *J. Geophys. Res., 104*, 4485, 1999.

Ma, Z. W., and A. Bhattacharjee, Sudden enhancement and partial disruption of thin current sheets in the magnetotail due to Hall MHD effects, *Geophys. Res. Lett., 25*, 3277, 1998.

Maynard, N. C., W. J. Burke, E. M. Basinska, G. M. Erickson, W. J. Hughes, H. J. Singer, A. G. Yahnin, D. A. Hardy, and F. S. Mozer, Dynamics of the inner magnetosphere near times of substorm onsets, *J. Geophys. Res., 101*, 7705, 1996a.

Maynard, N. C., W. J. Burke, G. M. Erickson, E. M. Basinska, and A. G. Yahnin, Magnetosphere-ionosphere coupling during substorm onset, in *Substorms 3, Eur. Space Agency Spec. Publ., ESA SP-339*, 301, 1996b.

Maynard, N. C., et al., Geotail measurements compared with the motions of high-latitude auroral boundaries during two substorms, *J. Geophys. Res., 102*, 9553, 1997.

Maynard, N. C., G. M. Erickson, W. J. Burke, A. G. Yahnin, J. C. Samson, G. D. Reeves, M. Nakamura, and V. V. Klimenko, Substorms and the inner magnetosphere: Onset and initial expansion, in *Polar Cap Boundary Phenomena, NATO Adv. Stud. Ser.*, edited by J. Moen, A. Egeland, and M. Lockwood, pp. 381–392, Kluwer Acad., Norwell, Mass., 1998a.

Maynard, N. C., G. M. Erickson, W. J. Burke, and G. R. Wilson, Magnetospheric electric fields during substorm onset and expansion phases, in *Substorms 4*, edited by S. Kokubun and Y. Kamide, pp. 605–610, Kluwer Acad., Norwell, Mass., 1998b.

McPherron, R. L., C. T. Russell, and M. P. Aubry, Satellite studies of magnetospheric substorms on August 15, 1968: Phenomenological models for substorms, *J. Geophys. Res., 78*, 3131, 1973.

McPherron, R. L., T. Terasawa, and A. Nishida, Solar wind triggering of substorm expansion onset, *J. Geomagn. Geoelectr., 38*, 1089, 1986.

Miura, A., S. Ohtani, and S. Tamao, Ballooning instability and structure of diamagnetic hydromagnetic waves in a model magnetosphere, *J. Geophys. Res., 94*, 15,231, 1989.

Moldwin, M. B., and W. J. Hughes, Geomagnetic substorm association of plasmoids, *J. Geophys. Res., 98*, 81, 1993.

Nagai, T., and S. Machida, Magnetic reconnection in the near-Earth magnetotail, in *New Perspectives on the Earth's Magnetotail, Geophys. Monogr. Ser.*, vol. 105, edited by A. Nishida, D. N. Baker, and S. W. Cowley, pp. 211–224, AGU, Washington, D.C., 1998.

Nakamura, R., D. N. Baker, T. Yamamoto, R. D. Belian, E. A. Bering III, J. R. Benbrook, and J. R. Theall, Particle and field signatures during pseudobreakup and major expansion onset, *J. Geophys. Res., 99*, 207, 1994.

Ohtani, S., and S. Tamao, Does the ballooning instability trigger substorms in the near-Earth magnetotail?, *J. Geophys. Res., 98*, 19,369, 1993.

Ohtani, S., K. Takahashi, L. J. Zanetti, T. A. Potemra, R. W. McEntire, and T. Iijima, Initial signatures of magnetic field and energetic particle fluxes at tail reconfiguration: Explosive growth phase, *J. Geophys. Res., 97*, 19,311, 1992.

Ohtani, S., F. Creutzberg, T. Mukai, H. Singer, A. T. Y. Lui, M. Nakamura, P. Prikryl, K. Yumoto, and G. Rostoker, Substorm onset timing: The December 31, 1995 event, *J. Geophys. Res., 104*, 22,713, 1999.

Olson, J. V., Pi2 pulsations and substorm onsets: A review, *J. Geophys. Res., 104*, 17,499, 1999.

Orr, D., and M. Cramoysan, The location of substorms using mid-latitude magnetometer arrays, in *Substorms 2*, pp. 435–438, Geophys. Inst., Univ. of Alaska Fairbanks, Fairbanks, Alaska, 1994.

Pu, Z. Y., A. Korth, Z. X. Chen, R. H. W. Friedel, Q. C. Zong, X. M. Wang, M. N. Hong, S. Y. Fu, Z. X. Liu, and T. I. Pulkkinen, MHD drift ballooning instability near the inner edge of the near-Earth plasma sheet and its

application to substorm onset, *J. Geophys. Res., 102*, 14,397, 1997.

Pulkkinen, T. I., Pseudobreakups or substorms, in *Substorms 3, Eur. Space Agency Spec. Publ., ESA SP-389*, 285, 1996.

Rostoker, G., Triggering of expansive phase intensifications of magnetospheric substorms by northward turnings of the interplanetary magnetic field, *J. Geophys. Res., 88*, 6981, 1983.

Rostoker, G., On the place of the pseudo-breakup in a magnetic substorm, *Geophys. Res. Lett., 25*, 217, 1998.

Rostoker, G., and J. V. Olson, Pi2 micropulsations as indicators of substorm onsets and intensifications, in *Auroral Processes*, edited by C. T. Russell, pp. 3–15, Jpn. Sci. Soc. Press, Tokyo, 1979.

Roux, A., S. Perraut, P. Robert, A. Morane, A. Pedersen, A. Korth, G. Kremser, B. Aparicio, D. Rodgers, and R. Pellinen, Plasma sheet instability related to the westward traveling surge, *J. Geophys. Res., 96*, 17,697, 1991.

Russell, C. T., and R. L. McPherron, The magnetotail and substorms, *Space Sci. Rev., 15*, 205, 1973.

Sergeev, V. A., T. I. Pulkkinen, R. J. Pellinen, and N. A. Tsyganenko, Hybrid state of the tail magnetic configuration during steady convection events, *J. Geophys. Res., 99*, 23,571, 1994.

Sergeev, V. A., V. Angelopoulos, D. G. Mitchell, and C. T. Russell, In situ observations of magnetotail reconnection prior to onset of a small substorm, *J. Geophys. Res., 100*, 19,121, 1995.

Shiokawa, K., W. Baumjohann, and G. Haerendel, Braking of high-speed flows in the near-Earth tail, *Geophys. Res. Lett., 24*, 1179, 1997.

Shiokawa, K., G. Haerendel, and W. Baumjohann, Azimuthal pressure gradient as driving force of substorm currents, *Geophys. Res. Lett., 25*, 959, 1998.

Singer, H. J., W. P Sullivan, P. Anderson, F. Mozer, P. Harvey, J. Wygant, and W. McNeil, Fluxgate magnetometer instrument on CRRES, *J. Spacecr. Rockets, 29*, 599, 1992.

Siscoe, G., Recent activity in substorm research, *Adv. Space Res., 13*(4), 165, 1993.

Siscoe, G. L., and W. D. Cummings, On the cause of geomagnetic bays, *Planet. Space Sci., 17*, 1795, 1969.

Vasyliunas, V. M., Theoretical considerations on where a substorm begins, in *Substorms 4*, edited by S. Kokubun and Y. Kamide, pp. 9–14, Kluwer Acad., Norwell, Mass., 1998.

Weimer, D. R., J. D. Craven, L. A. Frank, W. B. Hanson, N. C. Maynard, R. A. Hoffman, and J. A. Slavin, Satellite measurements through the center of a substorm surge, *J. Geophys. Res., 99*, 23,639, 1994.

Wygant, J. R., P. R. Harvey, F. S. Mozer, N. C. Maynard, H. Singer, M. Smiddy, W. Sullivan, and P. Anderson, The CRRES electric field/Langmuir probe instrument, *J. Spacecr. Rockets, 29*, 601, 1992.

Yahnin, A., et. al., Features of steady magnetospheric convection, *J. Geophys. Res., 99*, 4039, 1994.

Yeoman, T. K., H. Lühr, R. W. H. Fiedel, S. Coles, M. Grandé, C. H. Perry, M. Lester, P. N. Smith, H. J. Singer, and D. Orr, CRRES/ground-based multi-instrument observations of a substorm expansion phase onset, in *Substorms 2*, pp. 627–633, Geophys. Inst., Univ. of Alaska Fairbanks, Fairbanks, Alaska, 1994.

W. J. Burke and M. A. Heinemann, Air Force Research Laboratory, 29 Randolph Road, Hanscom AFB, MA 01731-3010. (burke@plh.af.mil; heinemann@plh.af.mil)

G. M. Erickson, Center for Space Physics, Boston University, 725 Commonwealth Ave., Boston, MA 02215. (ericksong@plh.af.mil)

N. C. Maynard and G. R. Wilson, Mission Research Corporation, One Tara Boulevard, Suite 302, Nashua, NH 03062. (nmaynard@mrcnh.com; gwilson@mrcnh.com)

(Received November 19, 1999; revised May 17, 2000; accepted May 24, 2000.)